Università degli Studi di Siena

DOCTORATE IN GENETICS, ONCOLOGY AND CLINICAL MEDICINE

CRISPR/Cas9-based Targeted Genome Editing for the Treatment of CDKL5 Deficiency Disorder

A thesis submitted for the degree of

Doctor of Philosophy

Supervisor:

Ilaria Meloni

Candidate:

Miriam L. Carriero

Doctorate Coordinator:

Francesca Ariani

March 2022

Digita qui il testo

Giuseppa Lucia Cerniglia

17/03/2022

Summary

List of Figures

List of Tables

Abstract

Mutations in the X-linked cyclin-dependent kinase-like 5 (*CDKL5*) gene cause CDKL5 deficiency disorder (CDD), which is a rare neurodevelopmental disease characterized by severe epilepsy and global developmental delay. Most children affected suffer from seizures beginning in the first months of life and severe impairment of cognitive and motor skills, with great impact on their quality of life. Most cannot walk, talk, or feed themselves, and many are confined to using a wheelchair. Although rare, CDKL5 deficiency disorder is one of the most common forms of genetic epilepsy. Currently, there is no cure or effective treatment for CDD, hence the great urge to develop novel and effective therapeutic strategies.

Here, we present a methodology for the correction of a pathogenic variant in *CDKL5* (c.1090G>T (p.Glu364*)), using CRISPR/Cas9 genome editing technology in patient-derived cell models, in order to expedite the discovery of new therapies for CDD.

CRISPR/Cas9 is a precise and versatile method of genetic manipulation, and it only requires three components to target and correct genetic mutations: guide RNAs, Cas9 endonuclease, and homology-directed repair (HDR) templates.

We first tested plasmid-based delivery of CRISPR/Cas9 for correction in primary fibroblasts. This system proved to be up to 66% efficient but it was associated with extremely variable and unpredictable editing efficiency (33±31%) in three separate experiments.

Hence, we decided to test additional guides and to replace the plasmid-based system with a protein-based ribonucleoprotein (RNP) delivery system for more rapid action and greater stability. We tested the system in induced pluripotent stem cells (iPSCs) obtained by reprogramming of the patient's fibroblasts. We reported the generation of genetically corrected iPSCs, where the mutated *CDKL5* c.1090G>T (p.Glu364*) was corrected to the wild-type, using RNP-mediated delivery of CRISPR/Cas9. Based on PCR cloning results of gene-corrected clones, we can state that our system is able to selectively target the p.Glu364* variant while preserving the wild-type *CDKL5* allele *in vitro*.

We then differentiated in parallel mutant and isogenic sets of cells into neural cells to assess the functional consequences of the edit in the affected cell type. We demonstrated that CRISPR/Cas9 gene editing restores the expression of CDKL5 protein in iPSC-derived neurons by Western blot. We also showed by RT-qPCR that mutant neurons carrying the c.1090G>T (p.Glu364*) in *CDKL5* present reduced expression of *CDKL5* mRNA compared to isogenic control.

Our findings demonstrate that we can achieve targeted and allele-specific correction of *CDKL5* (c.1090G>T (p.Glu364*)) variant using CRISPR/Cas9-RNP system in a patient-specific cell model. Moreover, we proved that correction of the mutation at the DNA level rescues CDKL5 protein expression and increase *CDKL5* mRNA expression in isogenic neurons.

The results of this study might be decisive in proving CRISPR/Cas9 potential to carry out genome editing in human cells, and ultimately for developing advanced therapies for CDD.

Introduction

CDKL5 deficiency disorder: an overview

CDKL5 deficiency disorder (CDD) is a rare genetic and chronically debilitating disorder characterized by early-onset infantile epileptic encephalopathy and severe neurodevelopmental delay, whose phenotype partially overlaps that of Rett syndrome (RTT, OMIM #312750) and X-linked infantile spasms (ISSX, OMIM #308350). For a long time, in fact, CDD was considered the early-onset seizure variant of RTT (ESV RTT), also known as the Hanefeld variant, more than a separate disease entity. It was first described in 1985 by Folker Hanefeld, a German physician who reported the case of a girl with atypical infantile spasms and delayed onset of symptoms consistent with classic RTT (1). The Hanefeld variant was later extended to include those with seizures of early onset (2).
RTT is a neurodevelopmental disease characterized by developmental regression with loss of motor, social, and communication skills. It may be variably accompanied by motor stereotypies, microcephaly, autonomic disorder, or epilepsy (3). Although it has been recognized that some alterations in initial development can be present, individuals with typical RTT do not have gross deviations in normal development in the first six to eighteen months of life (4). On the contrary, patients affected by the Hanefeld variant typically experience epileptic seizures at a very early stage between the first week and the first five months of life. In addition, retardation of psychomotor development is often observed already in the first months of life, without being preceded by a significant period of nearly normal development. In addition to the clear period of regression, these individuals also lack some other distinctive clinical features of RTT, such as the characteristic intense eye-gaze seen in individuals with typical RTT (5).
Besides early-onset seizures (before 5 months of age) and severe intellectual and gross motor impairment, diagnostic criteria for ESV RTT include infantile spasms, refractory myoclonic epilepsy, seizure onset before regression and decreased frequency of typical RTT (4). These clinical criteria were published by Neul in 2010 to differentiate the ESV from other atypical forms. Vegetative disorders, hand stereotypy, poor eye contact, breathing disorders, sleep disorders, and gastrointestinal problems, although less common, should also be considered in diagnosis (6–8). Nevertheless, the clinical picture of the disease is often heterogeneous, implying that significant phenotypic variation in patients should be taken into account (5).
It was not until 2003 that the Hanefeld variant was associated with the cyclin dependent kinase-like 5 gene (*CDKL5*), previously known as serine/threonine kinase 9 (*STK9*). The first *CDKL5* mutations were found in two girls with a West syndrome clinical picture (infantile spasms, hypsarrhythmia and severe mental retardation)(9). Shortly after, Weaving in 2004 and Scala in 2005 confirmed the occurrence of mutations in the *CDKL5* gene in patients previously diagnosed with the Hanefeld variant of Rett syndrome (10,11). In 2013, a large study conducted by Fehr exploited a large international data collection to describe the clinical profile of the CDKL5 disorder, comparing it with Rett syndrome (RTT). Since less than 25% of the analysed cases met the clinical criteria for ESV RTT, they concluded that it should not be considered part of the RTT spectrum anymore. The CDKL5 disorder became an independent entity, whose main hallmark feature was drug resistant early-onset epilepsy. Since then, a specific diagnosis of CDKL5-related disorder began to be used for individuals with mutations in *CDKL5* (12). In 2019, minimum diagnostic criteria for CDD were proposed to include the presence of a pathogenic or likely pathogenic variant in *CDKL5*, epilepsy onset within 1 year of age, and motor and cognitive delays (8) and CDD is currently treated as a separate disease entity.
Although rare, CDD is one of the most common causes of genetic childhood-onset epilepsy, with an estimated prevalence of one in 40,000 to 60,000 births (13,14).
Both cognitive impairment and refractory epilepsy in individuals with CDD are particularly severe, and case series suggest that symptoms are highly refractory to treatment (6,10,12). Like epilepsy, additional neurological symptoms negatively impact individuals' quality of life: most people affected cannot walk, talk, or feed themselves, and many are confined to a wheelchair. Due to the limited

therapeutic possibilities, patients with CDD may experience permanent symptoms of epileptic encephalopathy and significant developmental impairment (13,15). At the present time, there is no targeted therapy which could solve the underlying problem related to CDKL5 disorders and counter the primary pathology of these patients. Current therapeutic methods in patients with CDD are based on symptomatic drugs used to control or ameliorate the secondary symptoms of the disease, in particular, infantile seizures (16,17). Research is constantly being conducted to develop precise therapies based on the biological and genetic bases of CDD. The greatest hopes are placed in gene therapies as the only form of causal treatment of genetic disorders. The development of molecular and genetic therapies would thereby represent an important achievement in the field of public health and a much-needed response to the high demand for innovative therapies.

CYCLIN-DEPENDENT KINASE-LIKE 5 (CDKL5)

The human *CDKL5* gene is located on the short arm of the X chromosome, and it is subject to X-chromosome inactivation (XCI). Predictably, affected patients are almost always heterozygous females, with a prevalence of the disease four times higher among women than in men. All reported mutations thus far have dominant effects on phenotype (18). Like many other X-linked conditions, however, the course of the disease is usually more severe among hemizygous male patients (17).
The *CDKL5* gene occupies 228 kb of the Xp22 region and it codes for a serine/threonine kinase with a highly conserved N-terminal catalytic domain (residues 1–297), homologous to members of the mitogen-activated protein (MAP) kinase and cyclin-dependent (CDK) kinase families, and a long but much more poorly characterised C-terminus. The gene contains 27 exons which are combined in various transcript isoforms containing distinct coding regions, whereas the first exons (exons 1 to 1e) are untranslated. Five major transcript isoforms of *CDKL5* resulting from alternative splicing are known, including the two main known CDKL5 protein isoforms: one strongly expressed in the brain (hCDKL5_1; previously known as CDKL5107) and another only detected in testis (hCDKL5_5; previously known as CDKL5115) (18) (Fig. 1).

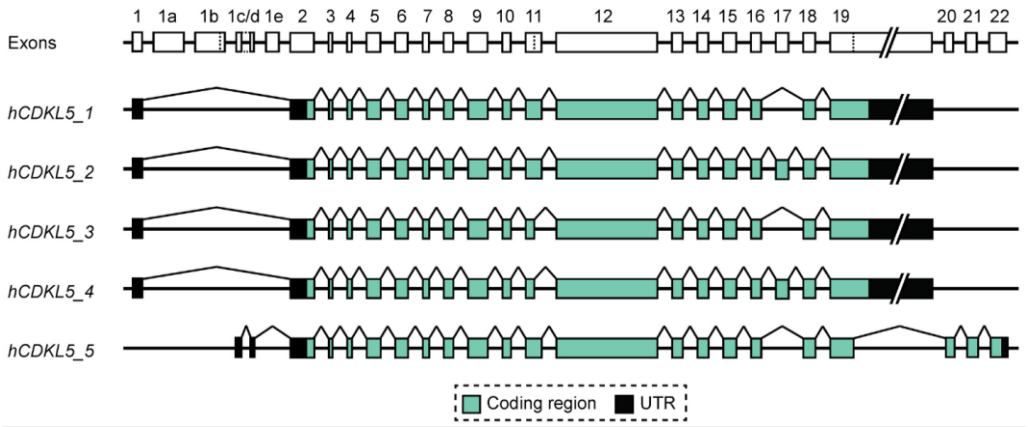

Figure 1

Human CDKL5 gene and transcript isoforms. *Diagram depicting the structure of the human CDKL5 gene and the exon composition of the five different coding isoforms, including hCDKL5_1 and hCDKL5_5. Lines linking exons indicate splicing events. Dotted lines within exons indicate alternative splice sites. (Hector RD et al., Characterisation of CDKL5 Transcript Isoforms in Human and Mouse. PLoS ONE. 2016).*

The *hCDKL5_5* transcript was the first to be reported and studied, and it generates a long protein of 1030 amino acids abundantly expressed in testis (9,18,19). This isoform uses a non-canonical polyadenylation signal downstream of the stop codon in exon 22, differentiating itself for the composition of the C-terminal region of the protein and of the 3'-UTR. The hCDKL5_1, formed by 960 residues, was later found to be the most abundant expressed isoform in the central nervous system (CNS), but it is also expressed in a wide range of tissues. This novel protein isoform is more stable and less prone to degradation through the proteasome pathway (20).
The differing molecular weight (107kDa and 115kDa) results from the different C-terminal regions that, although poorly characterized, are most certainly involved in regulation of the catalytic activity, localization, and protein-protein interaction (21–23).
All known CDKL5 isoforms appear to include a highly conserved serine/threonine kinase domain (residues 131–143), highly similar to those of MAP kinases and CDK families (24), and the ATP binding region (residues 19–43), located in the N-terminal half of the protein. The catalytic domain has a characteristic 12-subdomain structure of Ser/Thr kinases, highly conserved among many species (9,25). Between subdomains VII and VIII of the catalytic domain is present an activation loop whose autophosphorylation is known to activate CDKL5 catalytic functions. The activation loop includes the Thr-Xaa-Tyr (TEY) motif also observed in other kinases, such as the MAP kinase family (22,25,26). Two nuclear localisation signals (NLS) and a nuclear export signal (NES) are contained in the C-terminus of CDKL5 and were demonstrated to regulate intracellular localization of the protein (27,28) (Fig. 2).

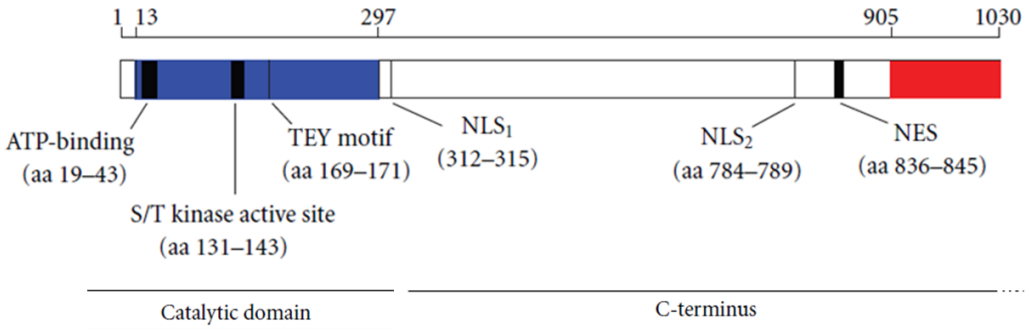

Figure 2

Schematic representation of hCDKL5_5. *Functional domains and signatures are indicated. NLS: nuclear localization signal; NES: nuclear export signal. (Kilstrup-Nielsen C et al., What We Know and Would Like to Know about CDKL5 and Its Involvement in Epileptic Encephalopathy. Neural Plasticity. 2012).*

The early postnatal onset of symptoms and the evidence that CDKL5 expression in the brain has a peak in early postnatal life suggests that CDKL5 plays a crucial role in brain development (18,29) CDKL5 is also expressed within the mature adult nervous system (21), where the protein exerts a role in cell proliferation and death, neuronal migration, axonal outgrowth, dendritic architecture, spine morphogenesis, and synapse development and function in the adult brain (30). Ricciardi in 2009 observed a novel and unexpected role of CDKL5, suggesting that CDKL5 may alter RNA processing and splicing regulation of several genes that would be particularly deleterious for the maturation, function or survival of brain neurons (31).
CDKL5 is expressed both in the nucleus and the cytoplasm of the cell soma and in dendrites. It shuttles between the two cellular compartments and the relative concentrations in each compartment seem to vary in different brain areas and during development (18). The C-terminal region of CDKL5, which is frequently deleted in pathogenic mutations, is believed to be involved in an active nuclear export mechanism modulating the subcellular distribution of the kinase (21).

It is widely assumed that in most cases CDD-related clinical symptoms result from loss of functions mutations of *CDKL5* resulting in the presence of non-functional CDKL5 protein or its complete absence. Most cases of CDD are the result of de novo mutations, however, cases of family history of *CDKL5* mutations were also reported, probably as a consequence of germline mosaicism in one of the parents (10,17).
Several mutation types and locations within the *CDKL5* sequence have been reported (missense, splicing, deletions/insertions leading to frameshifts and premature truncation) (5), but only one recurrent mutation (p.Ala40Val) has been so far identified (32). Disease-causing mutations are distributed in both the catalytic domain and the large C-terminal domain, suggesting that they are both important for CDKL5 function (Fig. 3). Missense mutations generally localize in the catalytic domain, while small deletions and non-sense or splicing mutations can be located anywhere in the gene, resulting in truncated proteins of various lengths (22,33).

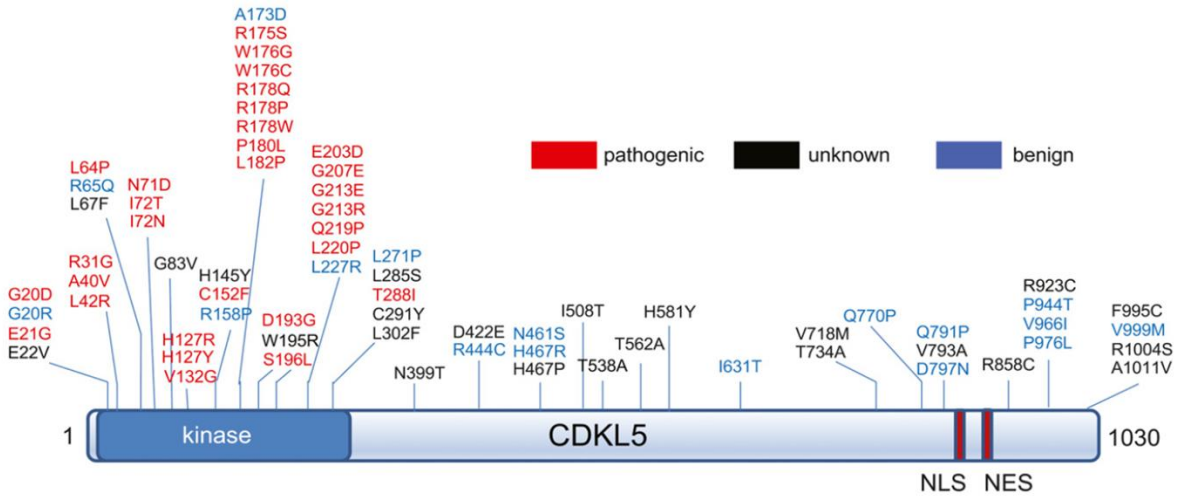

Figure 3

Pathogenic and non-pathogenic CDKL5 variants. *Schematic diagram shows the position of CDKL5 variants in humans that are either pathogenic, non-pathogenic or of unknown consequence according to RettBASE. NES: nuclear export signal; NLS: nuclear localization signal. (Muñoz IM et al., Phosphoproteomic screening identifies physiological substrates of the CDKL5 kinase. EMBO Journal. 2018)*

More than the nature or the position, however, the functional transcriptional and/or translational consequences of *CDKL5* mutations seem to correlate with the phenotypic heterogeneity of the disease and it could be speculated that the severity could depend on the proportion of functional CDKL5 produced by the mutated alleles (5).
CDKL5 premature termination codons (PTCs) correspond roughly to 15% of all mutations (16). These mutants create a premature stop codon predicted to generate a truncated CDKL5 protein lacking a large part of the C-terminal region. These truncated proteins, whereas they were produced *in vivo*, could have different abnormal functional consequences. Indeed, truncations of the C-terminus seem to enhance autophosphorylation and catalytic activity of CDKL5 and to cause atypical accumulation into the nucleus (21,22).
Although termination suppression by translational read-through of PTCs, resulting in continuation of transcription beyond the stop signal, is possible, transcripts containing PTCs are more likely to be degraded by nonsense mediated mRNA decay pathway (NMD)(34,35).

CRISPR/Cas9 genome editing technology

History and biology of CRISPR/Cas systems

The first targeted genome editing was produced in the 1970s and depended on the process of Homologous Recombination (HR), which was remarkably precise but very inefficient (36–39). The current genome editing technologies exploit three powerful classes of nucleases that can be programmed to make double-stranded DNA (dsDNA) breaks (DSBs) at essentially any desired target: Zinc-Finger Nucleases (ZFNs), Transcription Activator-Like Effector Nucleases (TALENs) and CRISPR (Clustered Regularly Interspaced Short Palindromic Repeats)/Cas (CRISPR-associated) (40). The CRISPR/Cas genome editing tools have been adopted rapidly in the research community and they now dominate in research laboratories around the world.
The first step in the timeline of CRISPR/Cas and genome engineering was the discovery in the late '80s of clusters of short repeats in the genome of Escherichia Coli (41). Those short spacer sequences interspersed with identical repeats were found to match viral genomes and were proposed to be part of an adaptive defence system, later precisely called Clustered Regularly Interspaced Short Palindromic Repeats (CRISPR)/Cas, that protects Bacteria and Archaea from invading viruses and plasmids (42). Cas genes encode CRISPR-associated proteins with nuclease and helicase domains, that can mediate capture, cleavage and inactivation of invading viral genomes, guided by short CRISPR RNAs (crRNAs) transcribed from the CRISPR arrays (43). The process occurs in three stages: first, in response to viral or plasmid challenge, a short sequence of the invading DNA (protospacer) is inserted into the host genome at the CRISPR array site; then the transcription of precursor crRNA (pre-crRNA) takes place and the pre-crRNA undergoes maturation to generate crRNAs (each composed of a repeat-spacer element and a targeting spacer portion); finally Cas proteins mediate the crRNA-directed cleavage of foreign nucleic acid at sites complementary to the crRNA spacer sequence (42,44,45).
There are three types of CRISPR/Cas systems, which use distinct molecular mechanisms for the processing of the pre-crRNA transcript. While in type I and type III systems this process requires a specialized endonuclease, type II system process pre-crRNAs by a different mechanism in which a separately encoded trans-activating crRNA (tracrRNA) complementary to the repeat sequences in pre-crRNA and a cellular RNAse III are involved (42,46). Cas9 endonuclease family, the hallmark proteins of Type II system, can be programmed with single RNA molecules (tracrRNA and crRNA) to cleave target dsDNA, a property that is extremely useful for genome engineering applications. Site-specific cleavage is also determined by the protospacer adjacent motif (PAM), a short motif juxtaposed to the complementary region in the target DNA (Fig. 4).

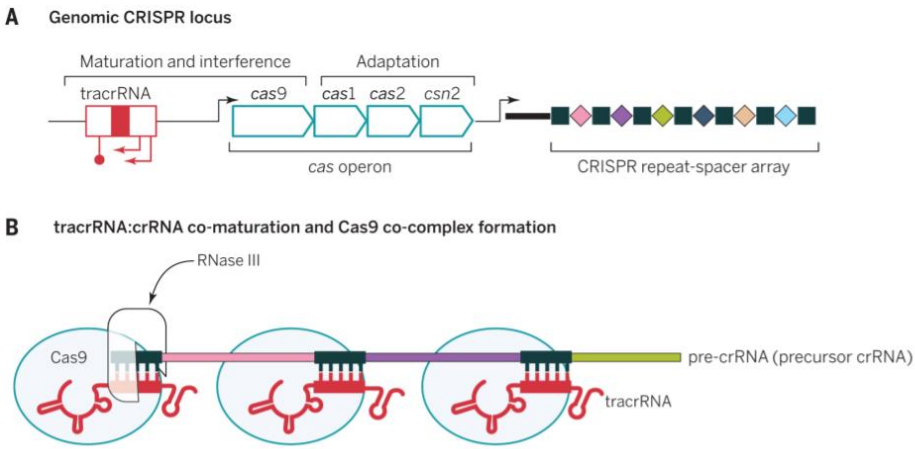

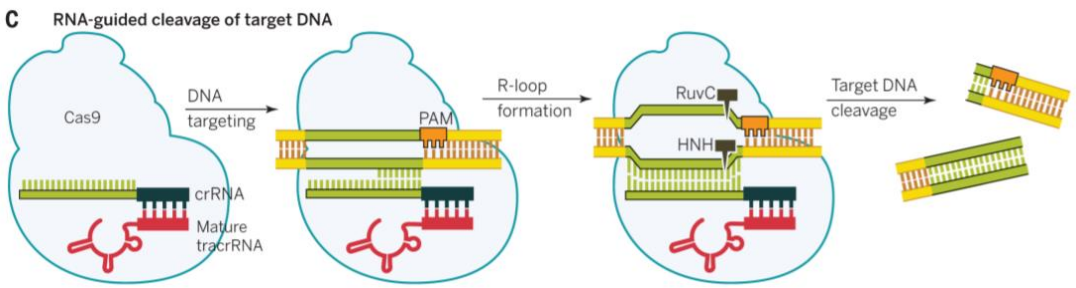

Figure 4

Biology of CRISPR/Cas9 system. (A) *The cas gene operon with tracrRNA and the CRISPR array.* ***(B)*** *The natural pathway of adaptive defense system against invading viral genomes involves association of Cas9 with tracrRNA: crRNA duplexes, RNA co-processing, loop formation, and target DNA cleavage.* ***(C)*** *Details of the natural DNA cleavage with the duplex tracrRNA:crRNA. (Doudna JA, Charpentier E. The new frontier of genome engineering with CRISPR-Cas9. Science. 2014).*

Since the beginning of 2013, in response to the exciting possibility of developing a simple and versatile RNA-directed system to generate DSBs for genome targeting and editing, laboratories around the world have used CRISPR/Cas9 to modify genes in a wide range of cell types and organisms, including human cells (42,45,47,48). CRISPR has been and continues to be a widely-used tool in research, with powerful applications across all branches of biotechnology, from basic science to engineering, as well as in commercial and human therapeutic applications (44,45). The first example of medical applications is the study of the development and progression of cancers and other diseases (including cardiovascular, metabolic and neurodegenerative diseases) or disease modelling, made possible by the precise reproduction of disease-associated genetic abnormalities, with the generation of human cell lines and primary cells bearing genetic aberrations resembling those described in the disease (49–54). CRISPR/Cas is also largely employed for genome-wide studies and systematic analysis of gene functions in mammalian cells that enable large-scale genetic screening for drug targets and other phenotypes (55,56). Another great potential of this technology is that it can be used for human gene therapy to treat genetic disorders. The ability of CRISPR/Cas system to correct genetic mutations responsible for inherited disorders represents a huge asset for human health and therapeutics.

In particular, genome manipulation in human induced pluripotent stem cells (hiPSCs), especially when they are derived in culture from somatic cells of an affected individual, allows generation of isogenic gene-corrected cell lines that can be used as very specific controls. This is most important when it comes to neurological disorders, where accessibility of the primarily affected cell type is challenging to say the least. For such diseases, CRISPR/Cas9 offer opportunities to develop *in vitro* human disease models that would recapitulate the relevant disease phenotype and provide a platform for drug screening and genetic studies (57–59).

RNA-programmable Cas9-mediated editing has been successfully applied to various mammalian cells, including human cells and embryonic stem cells (47,48,60–62), and at least two somatic therapies that involve genome editing using CRISPR/Cas9 have been approved (63,64). Previous results from CRISPR/Cas9 clinical trials proved that the technique can be successfully used to edit somatic cells *ex vivo*, through removal, editing and re-engraft of cells back into the patient (65,66). To be able to edit genes directly in the body (*in vivo* editing therapy), however, would require systemic or local delivery by viral or nonviral approaches and direct injection into the patient, opening the door to treating a wider range of diseases (67,68).

Engineering CRISPR/Cas systems: from theory to practice

The great merit of the genome editing nucleases is to make a targeted and thus very specific break in chromosomal DNA, but everything that happens after the break depends on cellular DNA repair machinery. The two major pathways of the DSB repair machinery are homology-dependent repair (HDR) in which a donor sequence matching the target is copied, and non-homologous end-joining (NHEJ) in which putting ends back together can lead to mutations at the break site (40).
The earliest studied and most common HDR pathway is HR. HR can use an unbroken sister chromatid or homologous chromosome as a template to precisely reconstruct the cleaved DNA, and it can be used to introduce specific point mutations or to insert desired sequences when supplied with exogenous DNA "donor templates" (69). On the contrary, NHEJ can lead to the introduction of insertion/deletion mutations (indels) of various lengths, which can disrupt the sequence of the gene. If NHEJ repair is acceptable when knocking out a target gene, it surely doesn't allow for integration of precise sequences. HR offers more precision than NHEJ and makes exact integrations without indels; its utility, however, is heavily limited due to its inefficiency, and NHEJ dominates DSB repair in many situations (70–72).
A way to influence the efficiency of homology-dependent events is through the design of the optimal DNA donor template. The distance of the intended DSB site from the Cas9 cut site, the type of HDR modification, the length of homology arms (HA), and the disruption of the CRISPR targeting site must be considered when designing DNA donor templates for use with the CRISPR/Cas9 system (40). Single-stranded (ssDNA) synthetic DNA oligo templates are commonly used for small modifications, such as single nucleotide (nt) change, knock-in of short sequences, or insertion of exogenous DNA up to ~100 nts. The insertion site and the DSB should be within ten nucleotides from one another, as HDR efficiencies quickly drop when this distance increases. Finally, in addition to the 20 bp to be bound by the guide RNA (gRNA), there must be an appropriately located PAM, which is an essential targeting component and can be used as a recognition system to prevent the CRISPR locus itself from being targeted (73).

Implementing this system in a given organism requires appropriate reconstitution of the functional crRNA-tracrRNA (trans-activating CRISPR RNA)-Cas9 functional unit. This involves expression of a Cas9 protein with an appropriate nuclear localization signal, and the crRNA and tracrRNA expressed either individually or as a single guide RNA (sgRNA) (48). There are three main strategies that have been developed for the delivery of CRISPR/Cas9 editing reagents: use of plasmids to encode Cas9 protein and gRNA (47,48), direct delivery of Cas9 messenger RNA (mRNA) and gRNA (74), and direct delivery of Cas9 protein and gRNA (75). The plasmid-based strategy requires the introduction of the encoded plasmid into the nucleus of the target cells where transcription takes place. Next, Cas9 mRNA and gRNA are exported from the nucleus to the cytoplasm where Cas9 mRNA is translated into protein and folded. The Cas enzyme and the gRNA bind to form a ribonucleoprotein (RNP) and are transported back into the nucleus where genome editing occurs. Each one of these steps represents a challenge in this system and plasmid-based delivery can result in variable editing efficiencies because of the uncontrollability of gRNA and Cas enzyme expression levels. Moreover, the plasmid-based genome editing exhibits greater stability but, precisely because of this, has also a greater propensity for off-target effects (OTEs) due to the longer lasting expression of Cas9 and gRNA that remain active in the cells for prolonged periods (74,75).
In contrast, the greatest drawback of direct delivery of Cas9 mRNA lies in the poor stability of mRNA, which results in transient expression limiting the duration of gene editing. On the bright side, it also reduces OTEs and toxicity (74).
Finally, the direct delivery to the target cells of Cas9 protein in complex with gRNA in a ribonucleoprotein (RNP) avoids many of the abovementioned complications. This alternative approach has several advantages, including rapid action, great stability, limited antigenicity and low toxicity (76). When pre-formed RNP is introduced into cells, in fact, the enzyme rapidly starts cutting targeted genomic DNA. Moreover, if the delivery is combined with cell-type specific reagents, the RNP is

directly transferred into the nucleus, with efficient transfection of even non-dividing cells. Using RNPs can also alleviate difficulties with protein expression that occur in cells after plasmid or mRNA delivery. On the negative side, many therapeutic targets cannot currently be accessed due to the lack of carriers that can deliver RNPs systemically; however, in adult mammals, recent studies have shown that RNP delivery *in vivo* is possible using nanoparticles (77).

Aim of the study

The overall objective of the proposed study was to develop a genetic therapy for CDD aimed to correct a pathogenic heterozygous variant in *CDKL5* (c.1090G>T (p.Glu364*)) using CRISPR/Cas9 technology, and to validate the system in a patient-specific cell model.

In particular, the specific aims of the project were:

1. Design of CRISPR/Cas9-based tools and reagents (including the screening process of candidate crRNAs) for targeted gene editing through HDR.
2. Generation of patient-derived cell models providing accurate representation of the affected individual genetic background.
3. Development of strategies for CRISPR delivery *in vitro* and for subsequent screening of gene-targeted cells.
4. Generation of isogenic gene-corrected cell lines and demonstration of the functional consequences of the genome editing in the disease-specific cell type.

Materials and methods

Study subject and sample collection

A 14-year-old girl suffering from early infantile epileptic encephalopathy was evaluated by the Medical Genetics Unit of the University Hospital of Siena. She was diagnosed with CDD after direct sequencing analysis of the *CDKL5* gene. The patient exhibited a single heterozygous nonsense mutation at Xp22.13 within the exon 12 of *CDKL5* representing a UAA premature stop codon (c.1090G > T; p.E364X). This mutation has already been reported and is predicted to generate a truncated CDKL5 protein lacking a large part of the C-terminal region (78). The mutation was not detected in the parents.
The patient exhibits early onset epileptic encephalopathy (45 days of age), developmental delay, bruxism, sialorrhea, hyperventilation and some RTT-like features, such as severe psychomotor impairment and motor stereotypies.
After informed consent obtained from the parents, a punch biopsy was carried out in local anaesthesia to obtain full-thickness skin specimens. About 4-mm diameter cylindrical core of tissue sample from the forearm was yielded rotating a circular blade down through the epidermis, dermis, and superficial fat. The sample was stored in phosphate buffered saline (PBS) at room temperature and processed shortly after collection.

Isolation and culture of human skin dermal fibroblasts

Primary cultures of human fibroblasts were obtained by a non-enzymatic dissection method, as previously described (79). Briefly, 4-mm round skin tissue was excised, cut into small pieces with sharp edges using forceps and a scalpel with a sterile blade, and placed into two 60-mm tissue culture dishes, trying to space the pieces evenly apart onto the surface of the dish. Once the biopsy pieces were dry enough, 5 ml of medium was added to each dish (CHANG medium, Irvine scientific, supplemented with antibiotics). The dishes were then transferred to a cell culture incubator set at 37 °C, 5% CO2, changing medium every other day. When, after 2–4 weeks, fibroblasts outgrowing from the biopsy pieces reached 80% confluence, cells were washed with PBS, trypsinized with 2.5 ml of 0.25% trypsin/ EDTA for 5 min at 37 °C and plated into T-25 flasks containing 5 ml of medium, and further expanded. Cells were frozen overnight at −80 °C in freezing medium (DMEM, 10% DMSO) and stored in liquid nitrogen.

Human iPSC culture and neural differentiation

The hiPSC line used in our study was generated from the patient's dermal fibroblasts by the CIBIO Cell Technology Facility (Trento, Italy) using Sendai virus particles delivering Yamanaka factors (CytoTune™-iPS 2.0 Sendai Reprogramming Kit, Thermo Fisher Scientific). Cells were fully characterized by immunofluorescence and pluripotency test using Embryoid Body (EB) assay.
iPSCs were cultured on Matrigel-coated dishes (10 cm diameter, Corning) with mTeSR1 medium (Stem Cell Technologies). Medium was changed every day. Cells were split by incubation with 0.5 mM EDTA (Invitrogen) for 3 min at 37ºC and cell aggregates were plated on Matrigel-coated dishes and maintained in culture for subsequent passages. For cryopreservation, cells were resuspended in freezing medium (FBS, 10% DMSO), transferred to cryovials, frozen overnight at −80 °C and then stored into liquid nitrogen. For thawing, cryovials were warmed in a water bath at 37°C until the icy masses disappeared, and cell suspension was transferred to 15 mL centrifuge tubes and diluted by addition of 10 mL mTeSR-1 medium. Cells were pelleted by centrifugation (1200 rpm, 5 min), resuspended, and seeded onto matrigel-coated dishes.

iPSCs were differentiated into spherical neural masses (SNMs) containing neuroectodermal progenitors and then differentiated into neural cells in monolayer culture as previously described (80). Briefly, for differentiation, iPSC colonies were grown to near full confluence in a 10-cm dish, dissociated into clusters with 0.5 mM EDTA (Invitrogen) at 37ºC for 3 min and seeded in a full 96-well clear V-Bottom TC-treated microplate (Corning) in mTeSR1 medium supplemented with 10 µM ROCK inhibitor (Sigma). The microplate was then centrifuged at 800 rpm for 10 min to form Embryoid Bodies (EBs). The next day, EBs were transferred to a 60-mm bacterial dish and cultured in mTeSR1 medium for 24 hours more. The EBs were then grown in suspension for 10 days with Induction Medium (DMEM/F12, Neurobasal medium, 0.5% N2 supplement, 1% B27 supplement (Life, 17504-044), 1% penicillin/streptomycin (PenStrep), 1% Glutamax) supplemented with 10 µM basic FGF (b-FGF) every other day. Then, EBs were plated on matrigel-coated plates in Induction Medium, supplemented with b-FGF every other day. After 10 days expansion, neural rosettes and neural tube-like structures were mechanically isolated and cultured onto bacterial culture dishes containing the Induction medium supplemented with b-FGF to form SNMs. The SNMs were grown in suspension for 7 days and then the appropriate number of spheres was plated on matrigel-coated plates or coverslips and cultured for 28 days in the absence of bFGF for differentiation into neurons. For passaging, SNMs were mechanically fragmented into four to six pieces and expanded. Mechanically fragmented SNMs were washed in PBS, resuspended in cryopreservation medium (FBS, 10% DMSO) as described above, transferred to cryovials and frozen overnight at −80 °C. Cells were then stored into liquid nitrogen.

Test for absence of Sendai virus

Total RNA was isolated using GeneJET RNA Purification Kit (Thermo Fisher Scientific) and purified with DNAse treatment using Turbo DNA free kit (Invitrogen). 500 µg purified RNA was used to synthesize cDNA to a final dilution of 5 ng/ul using Transcriptor first-strand cDNA synthesis kit (Roche) according to the manufacturer´s protocol. PCR amplification of 1 µL of cDNA from the reverse transcription reaction was performed as follows: denaturation at 95°C for 30 s, annealing at 55-60°C for 30 s, elongation at 72°C for 30 s, number of cycles 35. The expression of the retroviral-derived reprogramming factors KOS (acronym for the genes Klf4, Oct3/4, Sox2), Kruppel Like Factor 4 (Klf4), Sendai virus (SeV), cMyc was analyzed by RT-PCR. Human *GAPDH* was used as internal control. Specific primers are listed in Table 1.

Table 1 *Primers for RT-PCR of Sendai virus derived pluripotency factors*

Gene	Forward primer	Reverse primer
SeV	5′-GGATCACTAGGTGATATCGAGC-3’	5′-ACCAGACAAGAGTTTAAGAGATATGTATC-3′
KOS	5′-ATGCACCGTACGACGTGAGCGC-3′	5′-ACCTTGACAATCCTGATGTGG-3′
Klf4	5′-TTCCTGCATGCCAGAGGAGCCC-3’	5′-AATGTATCGAAGGTGCTCAA-3’
cMyc	5′-TAACTGACTAGCAGGCTTGTCG-3’	5′-TCCACATACAGTCCTGGATGATGATG-3’

Karyotype analysis

Cells were treated with Colcemid® Solution (GIBCO) at a final concentration of 0,1µg/mL and incubated for 3 hours. Cells were harvested with tripsin/EDTA 0.05%. Cells were then suspended in prewarmed hypotonic solution (KCl 75mM) and incubated for 15 min at 37°C. Cells were fixed with fixative solution (methanol/glacial acetic acid 3:1). Chromosome spread and interpretation of

chromosome structure by G-band staining was performed by the certified laboratory of the “Hosp. Univ. Materno-infantil Sant Joan de Déu” (Esplugues de Llobregat, Spain). High quality chromosome spread for subsequent analysis of chromosome set by G-banding was obtained as previously described (81). Twenty metaphases were studied.

Mycoplasma testing

All cellular cultures were routinely tested for mycoplasma by PCR. Media supernatants were collected from confluent cultures and 100µl of each sample were used for PCR with the Venor®GeM Classic kit. The mycoplasma-specific amplification is detected at 265-278 bp. False negative results due to PCR inhibitors or improper DNA extraction were ruled out by using the provided internal amplification control, which is detected at 191 bp. Only negative samples were used in the study.

X chromosome inactivation (XCI) study

Genomic DNA was extracted using QIAmp DNA Mini Kit (Qiagen) following the standard extraction protocol. 500 ng of DNA was digested for 2 h at 37ºC with 10 U Hpa II (New England Biolabs). The digested DNA fragments were PCR-amplified for 35 cycles with 1 min denaturation at 95ºC, 30s annealing at 60ºC, and 30s extension at 72ºC. Non-digested DNA was amplified in parallel. The final selective amplification products were separated on 1.2% agarose gel and visualized by exposure to UV rays. The following primers were used: RS1: GCTGTGAAGGTTGCTGTTCCTCAT; RS2: TCCAGAATCTGTTCCAGAGCGTGC. RS1 was labelled with a fluorescent dye (5’-FAM) to allow PCR analysis by capillary electrophoresis separation. The loading mixture was prepared using 20µl formamide and 0.25µl of GeneScan LIZ dye size standard (Thermo Fisher Scientific) per sample. 1ul PCR products was added to the loading mixture. After incubation at 95 °C for 5 min, the denatured samples were loaded on an automatic sequencer (ABI PRISM® 3130 Genetic Analyzer, Applied Biosystems, Courtaboeuf, France) for analysis.

Sanger sequencing

Total RNA was extracted with RNAeasy Mini kit (Qiagen, Courtaboeuf, France) as described by the manufacturer. RNA quality was assessed with the NanoDrop Spectrophotometer. Reverse transcription of total RNA (1 µg/reaction) with elimination of genomic DNA was carried out with the QuantiTect Reverse Transcription Kit (Qiagen). Regions containing the mutations were PCR-amplified and sequenced with an ABI PRISM® 3130 Genetic Analyzer (Applied Biosystems, Courtaboeuf, France).

Plasmid vector construction

The genomic sequence was analysed to locate a PAM sequence in close proximity of the target site. A gRNA directed against the human *CDKL5* E364X variant and driven by the U6 promoter was engineered together with a dsDNA donor into the AflII and SacII restriction sites of the pAAV2.1 CMV/GFP3 vector plasmid (kindly provided by Dr. A Auricchio, Federico II University, Naples, Italy) (82). The gRNA consists of a 20-nt target sequence. The dsDNA donor template was created with 120 bp homology to the target site and a synonymous nucleotide change mutating the PAM sequence. The sequences are listed in Table 2 and the synonymous change in the donor template is highlighted in grey. To generate the plasmid for cloning a dual fluorescent protein reporter, the EGFP (enhanced green fluorescent protein) sequence of the pAAV2.1 CMV/GFP3 vector was extracted by

NheI and *SpeI* digestions and replaced by the mCherry-EGFP construct, resulting in the following plasmid: pAAV2.1 U6-gRNA-CDKL5. Finally, the target sequence (PAM+gRNA) was engineered into the *BsmBI* restriction site of the pAAV2.1 U6-gRNA-CDKL5 vector, into the mCherry-EGFP insert.
The pX551 (pAAV-pMecp2-SpCas9-spA) vector was used for the delivery of *Streptococcus pyogenes* Cas9 (spCas9) driven by *MECP2* promoter (83). The PAM sequence recognized by SpCas9 is NGG. The target sequence was engineered into the *AgeI* restriction site of the vector between Cas9 promoter sequence and CDS, to avoid long-term expression.
All plasmid constructs were generated by the Core Research Laboratory of the Institute for Cancer Research, Prevention and Clinical Network (ISPRO, Florence, Italy) and confirmed by sequencing.

Table 2 *Guide RNA and dsDNA sequences for plasmid construction*

Name	Strand	Sequence	PAM sequence	Promoter
gRNA	-	TCCATTTAGGAAGCTTTAAT	TGG	U6
dsDNA		AGGACATCCAGAACCTGAGTGTAG-GCCTGCCCCGGGCT-GACGAAGGTCTCCCTGCAAAT-GAAAGCTTCCTAAATGGAAACCTTGCTGGAGCTAGTCTTAGTCCACTGCACACCAAAACCT		CMV

Plasmid transfection and cell sorting

One million cells were co-transfected with a mix of 3 µg of the pAAV2.1 U6-gRNA-CDKL5 plasmid and 9 µg of the pX551 Cas9 expressing vector using the Neon Transfection System (Thermo Fisher Scientific) according to the manufacturer's instructions (1700V, 1 pulse, 20ms). Negative transfection controls obtained by transfection of empty vector were included. Cells were seeded on 60-mm tissue culture dish and incubated in antibiotic-free medium. After 24 hours, the medium was replaced by fresh complete medium. Cells cultured for a total of 48 hours after transfection were dissociated with Trypsin and the pellet was resuspended in PBS/EDTA 3mM and Trypsin 2%. A BD FACSAria II (BD Biosciences, USA) cell sorter was used for cell separation. Gating and data analysis were done with BD FlowJo v7.5 (BD Biosciences, USA) software. EGFP+ cells were collected into tubes containing 3 ml medium and kept on ice until the samples were processed for DNA isolation.

Next-generation sequencing

DNA was isolated using QIAamp DNA Micro Kit (QIAGEN, Hilden, Germany), according to manufacturer's instructions. Samples were processed using the commercially available Ion AmpliSeq 2.0TM Library Kit (Life Technologies), according to manufacturer's instructions, and sequenced on Ion Torrent S5 platform. Libraries were purified using Agencourt AMPure XP system and quantified using Qubit dsDNA HS Assay Kit reagent (Invitrogen Corporation, Life Technologies), pooled at an equimolar ratio, annealed to carrier spheres (Ion SphereTM Particles, Life Technologies), and clonally amplified by emulsion PCR using the Ion Chef system (Life Technologies). Ion 510TM, 520TM, or 530TM chips were loaded with the spheres carrying single stranded DNA templates and sequenced on the Ion Torrent S5 using the Ion S5TM Sequencing kit, according to the manufacturer's protocol. Integrative Genomics Viewer (IGV) Visualization Software (Broad Institute, Cambridge, USA) was utilized to analyse the data. For every sample, roughly 0.8–1.0-M raw reads were

generated. The rate of reads mapped to the genome was approximately 72.0%. The average sequencing depth per genome was 0.02.

crRNA selection

Three crRNAs targeting the c.1090G>T variant of the human *CDKL5* gene were selected using the Primer Blast online platform. The results were then cross-referenced with a number of other web tools for selecting target sites for CRISPR/Cas9, such as Benchling, CCTop, CHOP CHOP, and Integrated DNA Technologies (IDT). All PAMs were located in the middle of the targeted region close to the target site. Guides with the highest on-target and lowest off-target scores were selected. crRNAs were ordered from IDT (Table 3).

Table 3 *Guide RNAs*

Name	Position	Strand	Sequence 5'>3'	PAM sequence	GC content %	ON-target score	OFF-target score	Cutting site-mutation distance
gRNA1	1083-1102	-	TTAGGAAGCTTTAATTGGCA	GGG	35	57,6	48,5	4
gRNA2	1088-1107	-	TCCATTTAGGAAGCTTTAAT	TGG	30	21,7	54,4	0
gRNA3	1084-1103	-	TTTAGGAAGCTTTAATTGGC	AGG	35	45,8	61,6	3

HDR template design

A ssDNA template for HDR having HAs spanning 100 bp from both sides of the mutation site was designed. A single silent nucleotide change was introduced in the donor template to mutate the PAM sequence and block further editing after initial repair. The abovementioned mutation also removed a *BsaI* restriction digest site, thus altering the digestion profile of PCR products and allowing for the detection of HDR.

DNA cleavage by in vitro assembled Cas9 RNP complex

To prepare the crRNA-tracrRNA duplex, each crRNA and tracrRNA was reconstituted to 100 µM with Nuclease-Free Duplex Buffer (IDT). Oligos were mixed at equimolar concentrations to a final crRNA-tracrRNA duplex concentration of 10 µM and annealed by heating at 95°C for 5 min. The duplexes were complexed with spCas9 high-fidelity variant protein (Alt-R® S.p. HiFi Cas9 Nuclease V3, IDT) in equimolar amounts and incubated at room temperature for 10 min.
For *in vitro* digestion, linearized substrate DNA was prepared by PCR amplification of the target site. PCR primers CDKL5-2 (Table 4) were designed to produce an amplicon of 582 bp surrounding the desired crRNA cleavage site but with the target site off-center, in order to produce cleavage products of different sizes (325 bp and 256 bp, respectively) easily resolvable by gel electrophoresis. After incubation of the DNA substrate (100nM) with the RNP complex at 37°C for 60 min, 1 µL Proteinase K (20 mg/mL) was added to the reaction, followed by incubation at 56°C for 10 min to release the DNA substrate from the Cas9 endonuclease. Cleavage fragments from the digestion reactions were separated and analysed by gel electrophoresis. Densitometry analysis was performed with ImageJ.

Table 4 *Primers for amplification of genomic DNA*

	Sequence (5'->3')	Template strand	Length	Start	Stop	Tm	GC%	Self comple-mentarity	Self 3' comple-mentarity	Product length
CDKL5-1-FW	ATAGAAACCAAGCCGGCAAA	Plus	20	14	33	58.08	45.00	6.00	0.00	981
CDKL5-1-RV	TCAACTGTACCTGGGGTGAC	Minus	20	994	975	58.95	55.00	4.00	3.00	
CDKL5-2-FW	TTTCATCAAGGCCAGTGCTTT	Plus	21	108	128	58.68	42.86	4.00	3.00	582
CDKL5-2-RV	TCCATGAATGAGTGGCGGTT	Minus	20	689	670	59.67	50.00	4.00	0.00	

Cas9/RNP Nucleofection

iPSCs were dissociated into single cells from semiconfluent 10-cm dish with Accutase (LabClinics) at 37°C for 5 min, after 1h pre-incubation with 10 µM ROCK inhibitor. RNP mix was prepared by incubating the crRNA-tracrRNA duplexes (200pmol) with the Cas9 protein (40pmol) at room temperature for 10 min. Two hundred fifty thousand cells were resuspended in 20 µl P3 primary cell nucleofection solution (Lonza Bioscience) and mixed with 5 µl RNP. The cell/RNP mix was transferred to Nucleofection cuvette strips and electroporated using a 4D-Nucleofector (Lonza Bioscience), applying electroporation protocol CA137. After nucleofection, prewarmed medium supplemented with 10 µM ROCK inhibitor was used to transfer transfected cells in matrigel-coated 24-well plates.

Mismatch detection assay

Genomic DNA was extracted from transfected cells using QIAmp DNA Mini Kit (QIAGEN). Target regions were PCR-amplified (primers CDKL5-2, Table 4) with GoTaq G2 Flexi DNA Polymerase (Promega). PCR products were purified (DNA clean and concentrator Kit, Zymo Research) and run on a 1.2% agarose gel to check for the presence of a single band of expected size. PCR products were denatured at 95 °C for 10 min and re-annealed at −2 °C per second temperature ramp to 85 °C, followed by a −1 °C per second ramp to 25 °C (Table 5). The heterocomplexed PCR product (200 ng) was incubated with 1 ul T7 Endonuclease I enzyme (New England Bio Labs) at 37°C for 15 min. A negative control with untreated DNA was included. The products were run on 2% agarose gel and analysed as described above (see DNA cleavage by in vitro assembled Cas9 RNP complex).

Table 5 *T7EI assay hybridization conditions*

Step	Temperature	Ramp	Time
Denaturation	95°C		5 min
Annealing	95-85°C 85-25°C	-2°C/sec -0.1°C/sec	
Hold	4°C		Hold

Restriction enzyme digest

Genomic DNA was PCR-amplified (primers CDKL5-2, Table 4) The PCR products were incubated with High Fidelity *BsaI* restriction enzyme (High Fidelity version BsaI-HF®v2, NEB) at 37°C for 1 hour. The digestion was terminated by heat inactivation at 80°C for 20 min. A control reaction without the enzyme was included for each sample. Digestion products were run on 2% agarose gel and the restriction pattern was analysed.

Isolation of clonal cell lines

Nucleofection was performed as described above (see “Cas9/RNP nucleofection”) except that this time 100pmol ssDNA was added to the RNP/cell nucleofection mix.
After 3 days expansion, iPSCs were dissociated into single cells with Accutase (LabClinics) at 37°C for 5 min, and highly diluted in 30 ml medium. Cells were seeded at low density in matrigel-coated 10-cm dishes and further expanded to obtain single cell-derived clones, according to limiting-dilution cloning method. Once the colonies attained a certain size, they were mechanically isolated, sampled and further expanded. For clarity, the patient-derived and the genetically corrected cell clones are called mutant and corrected clones, respectively.

PCR cloning

Genomic DNA was amplified by PCR primed with oligonucleotide primers CDKL5-1 (Table 4) using high-fidelity Phusion polymerase. The size of the desired amplification product was analysed by electrophoresis on agarose gel. The PCR product was then cloned into a plasmid vector using TOPO® TA Cloning® Kit with pCR™ 2.1-TOPO® vector (Thermo Fisher Scientific). The recombinant vector was transformed into One Shot® Chemically competent cells following manufacturer’s instructions. Transformant colonies were selected monitoring the disruption of the X-gal gene on plating medium containing the chromogenic substrate X-gal and cultured overnight in LB medium containing 50 µg/mL ampicillin and supplemented with IPTG. Plasmid DNA was then isolated using GeneJET Plasmid Miniprep Kit (Thermo Fisher Scientific) and analysed by sequencing using primers CDKL5-1.

Quantitative real-time polymerase chain reaction

Total RNA was isolated from differentiated cells using GeneJET RNA Purification Kit (Thermo Fisher Scientific), and 1 µg was used to synthesize cDNA using Transcriptor first-strand cDNA synthesis kit (Roche) according to the manufacturer´s protocol. The quantitative real-time polymerase chain reaction (real-time RT-qPCR) was carried out with the SYBR® Green PCR Master Mix using the 7900 HT Fast Real-Time PCR System (Applied Biosystems). Gene expression was normalized to that of *GAPDH* as the internal control and quantified by the ΔΔCt method. Specific primers are listed in Table 6. Differences in gene expression level were calculated, and difference in means was tested by unpaired t test.

Table 6 *Primers for RT-qPCR*

Gene	Forward primer	Reverse primer
NMDAR1	5′-GTCCACCAGACTGAAGATTGTGAC-3’	5′-CTCCTCCTTGCATGTCCCA-3′
NMDAR2A	5′-GCTCTTCTCCATCAGCAGGG-3′	5′-GGATCCCGTCAGATTGAAGTCT-3′
GFAP	5′-CTCTCCCTGGCTCGAATG-3’	5′-GGAAGCGAACCTTCTCGATGTA-3’
MAP2	5′-ATGGGTCACAGGGCACCTATTCAA-3’	5′-TGCTGTTTCTCTGTCAGCTGAGGT-3’
GAD1	5′-ATCCTGGTTGACTGCAGAGAC-3’	5′-CCAGTGGAGAGCTGGTTGAA-3’
GAD2	5′-CTGCTCCAAAGTGGATGTCAAC-3’	5′-AAAGTGGGCCTTTCTCCATCA-3’
CDKL5	5′-AGAAGTTCTTTTGGTGCCATGT-3’	5′-AACTCCATAGGCTCCTTCACC-3’

Western blotting

The levels of CDKL5 protein were determined by Western blot analysis. Briefly, proteins were extracted from iPSCs and iPSC-derived neurons with RIPA lysis buffer (10mM Tris-HCl pH 8.0, 1mM EDTA, 0.5mM EGTA, 1% Triton X-100, 0.1% Sodium Deoxycholate, 0.1% SDS, 140mM NaCl). For quantitation, BSA standard curve was prepared as follows: BSA protein stock solution 0.5 mg/ml was made diluting BSA 1 mg/ml 1:2 in ultrapure water (Milli-Q) and pipetted in the 96-well plate as outlined in Table 7. A range of dilutions (1, 1/10, 1/20) of protein sample was assayed. 200ul protein assay dye reagent (Bio-Rad) diluted 1:5 in ultrapure water were added to each well. Samples and protein standards were made in triplicates. The A595 of the samples and protein standards against the blank reagent was measured 15 minutes after mixing. The protein samples (30 µg) were separated by electrophoresis on a precast polyacrylamide gel (Bolt™ 4-12% Bis-Tris Plus Gel, Invitrogen) and then transferred to a pre-cut nitrocellulose membrane (Invitrogen) using the iBlot™ 2 Gel Transfer Device (Invitrogen™). After blocking non-specific sites by a TBS-Tween 20 0.1%/fat milk 5% solution for 1 h at room temperature, the membrane was incubated overnight at 4°C with a rabbit anti-CDKL5 polyclonal antibody (Sigma-Aldrich; dilution 1:500), washed and incubated with a horseradish peroxidase (HRP)-conjugated anti-rabbit IgG (dilution 1:1000) and developed with the enhanced chemiluminescence method (ECL; GE Healthcare). Membranes probed for CDKL5 were reprobed for β-actin (dilution 1:5000) for loading normalization.

Table 7 *BSA standard curve*

Gene	Proteine concentration (mg/ml)	BSA sock (0.5 mg/ml)	H_2O Milli-Q
A	0.0	0 µl	10 µl
B	0.05	1 µl	9 µl
C	0.1	2 µl	8 µl
D	0.2	4 µl	6 µl
E	0.3	6 µl	4 µl
F	0.4	8 µl	2 µl
G	0.5	10 µl	0 µl

Immunofluorescence staining

8-week-old neurons seeded on matrigel-coated coverslips were fixed with 4% paraformaldehyde (PFA) for 15 min at room temperature. After three washes in 1X TBS (10 min each), samples were incubated in blocking solution (1X TBS, 0.5% Triton-X100 (Sigma) and 6% donkey serum) for 1 h at room temperature and incubated with primary antibodies diluted in TBS++ (1X TBS, 0.1% Triton-X100 and 6% donkey serum) overnight at 4ºC. After 3 washes in TBS++ (10 min each), samples were incubated with secondary antibodies diluted in TBS++ for 2 h in the dark at 37°C. Finally, coverslips were washed thrice with 1X TBS for 10 min each and incubated with DAPI (Invitrogen) for 10 min at room temperature. Coverslips were mounted onto microscope slides. Primary and secondary antibodies used are listed in Table 8.

Table 8 *Primary and secondary antibodies used for immunofluorescence*

Antibody	Source	Catalogue number	Dilution
Chicken anti-MAP2	Abcam	AB5392	1:1000
Rabbit anti-GFAP	Dako	Z0334	1:500
Rabbit anti-SYNAPSIN	Calbiochem	574777	1:200
Donkey anti-Chicken IgY-Alexa Fluor 488	Jackson	703-545-155	1:50
Donkey anti-Rabbit IgG-Alexa Fluor 647	Jackson	711-606-152	1:200

Image acquisition and analysis

Images were taken using an SP5 confocal microscope (Leica Microsystems) equipped with a 40x oil immersion objective. In all cases, the pinhole size was set at 1 AU and a frame size of 1024x1024 was used. Laser power, digital gain and digital offset were adjusted using the brightest specimen and kept constant across the acquisitions. Z-stacks were collected for three channels (GFAP, MAP2 and DAPI) covering the entire volume of the cell using a step size of 0,84µm. Random locations were acquired for subsequent image analysis. The images were imported into Imaris software to perform the image analysis. The Surface Imaris tool was used to create an isosurface for each channel. Fluorescence intensity was expressed as the ratio of intensity sum and surface volume. The information generated by Imaris was then exported to Excel for use.

Statistical analysis

The number of replicated measurements per experiment (n) and of independent experiments (N) is specified in the figure legends. Comparisons between experiments involving two groups with normal distribution were performed with unpaired *t* test using GraphPad Prism software to determine statistical significance. All values were expressed as the mean ± SD. A value of $p < 0.05$ was considered statistically significant.

Results

Characterization of iPSCs generated from patient-derived fibroblasts

A single heterozygous nonsense mutation in the *CDKL5* gene was found in a female subject by direct sequencing of genomic DNA. We established patient-derived primary fibroblasts culture from skin punch biopsy using a non-enzymatic dissection method previously described (79).
The iPSC line used in this study was generated from patient's dermal fibroblasts by the CIBIO Cell Technology Facility (Trento, Italy) using non-integrating Sendai virus particles delivery of the transcription factors Sox2, Klf4, Oct4, and c-Myc. Cells were fully characterized and positivity for pluripotency markers and multilineage differentiation potential were confirmed. However, no cytogenetic study or test for proof of absence of reprogramming factors were conducted ahead of delivery.
We initially noted extremely poor post-thaw recovery of cryopreserved iPSCs, resulting in low survival rate of the population and growth failure in culture. Finally, after one month of weekly passages using single cell dissociation, we were able to stably expand a single clone (clone U) which showed typical characteristics of human pluripotent stem cells and absence of spontaneous differentiation *in vitro* (Fig. 5 A). Contextually, post-thaw cell viability of cryopreserved iPSCs clone U greatly increased. Karyotype analysis of G-banded metaphase spreads from iPSCs clone U, however, revealed a complete trisomy of chromosome 8 (chromosomal formula: 47, XX, + 8) (Fig. 5 B). We reckon that poor post-thaw recovery, together with long-term culture, contributed to the genetic instability inherent in stem cell culture. It should be noted that at no time examination of cell culture showed changes in iPSC-like morphology. Given the difficulties in obtaining other stable clones, we decided to proceed with iPSC clone U despite the aneuploidy.

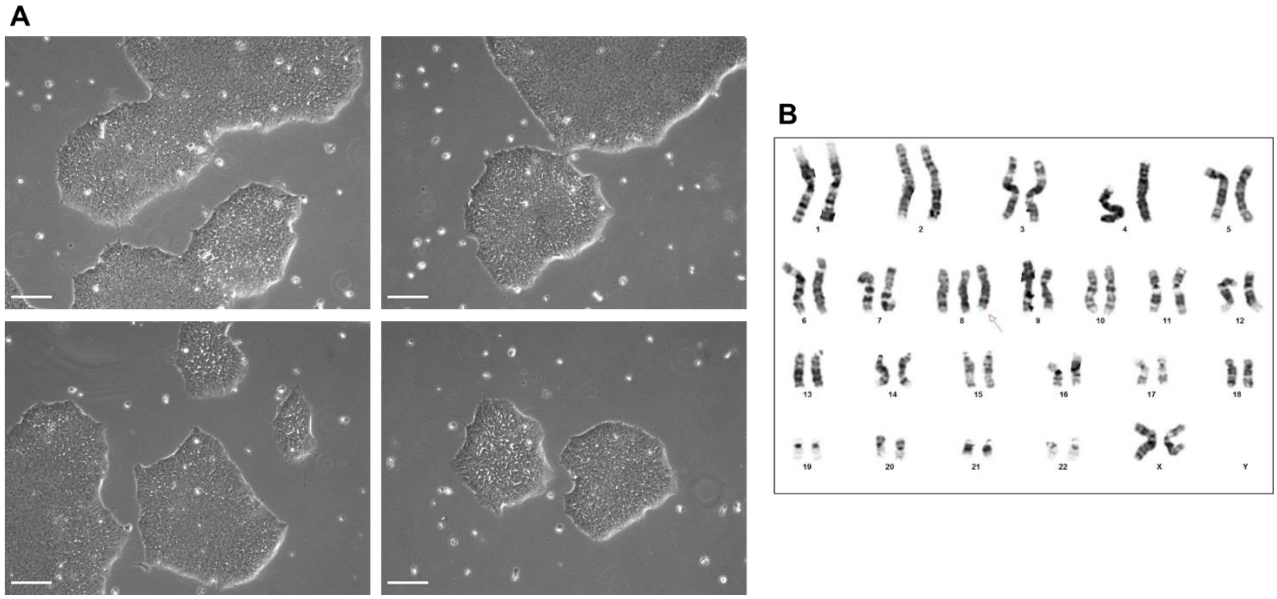

Figure 5

iPSCs morphology and chromosomal status. (A) *Representative images of iPSC (clone U) cultures showing medium- and large-sized colonies comprised of highly packed cells and well-defined borders. Scale bars = 100 µm.* ***(B)*** *Representative Giemsa-banded karyotype image of iPSC clone U at passage 20 showing trisomy of chromosome 8 in all 20 metaphases analysed (white arrow).*

Since delivery of the transcription factors Oct4, Klf4, Sox2 and c-Myc via non-integrating viral vectors can result in residual reprogramming transgene expression, altering the biological properties of iPSCs, we tested the cells to ensure the absence of reprogramming factors. We performed RT-PCR on total RNA isolated from iPSCs at passage 20 with primers specific for the transgenes and we demonstrated no residual persistent transgene expression (Fig. 6).

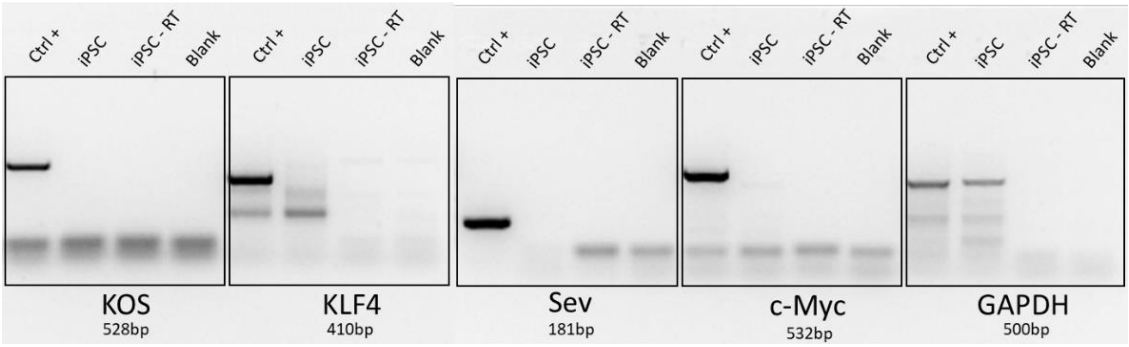

Figure 6

Analysis of Sendai viral transgene expression in iPSC line. *RT-PCR for the expression of the reprogramming vectors KOS (Klf4, Oct3/4, Sox2), Klf4 (Krüppel-like Factor 4), SeV (Sendai virus) and cMyc. Human GAPDH was used as internal control. From left to right, positive control, iPSC line, no reverse transcriptase control (-RT) and negative control (blank).*

iPSCs maintain X-inactivation upon reprograming of patient-derived fibroblasts

Since *CDKL5* is found on the X chromosome, and one of the two X chromosomes is randomly inactivated in females, only one of the *CDKL5* alleles is expressed from the active X chromosome in each cell. Hence, individual cells from CDD female patients either express the wild-type or the mutant allele (84). Consequently, somatic cells are usually mosaic for the inactive X chromosome (Xi).
We investigated X chromosome inactivation status in patient-derived fibroblasts by sizing the polymorphic CAG trinucleotide repeat of the *AR* gene, as previously described (85). After digestion with *HpaII*, only unmethylated DNA is digested, while methylated DNA is left intact. Therefore, PCR amplification will only occur if the restriction sites are methylated and resistant to restriction enzyme digestion (85). Non-digested DNA is amplified in parallel to identify AR alleles. Capillary electrophoresis analysis of the PCR products from *HpaII* digested and non-digested DNA showed extremely skewed X-chromosome inactivation in patient-derived fibroblasts (Fig. 7 A).
Sequencing analysis of the *CDKL5* transcript in fibroblasts revealed preferential expression of the mutated allele (Fig. 7 B).
To test whether iPSCs obtained by reprogramming of patient's fibroblasts preserved XCI, with one of the two X chromosomes exclusively being inactive, we analysed the *CDKL5* transcript sequence in 4 clones. Only iPSCs clones expressing the mutant allele and carrying the wild type allele on the inactive X chromosome were identified, in line with the preferential inactivation of the wild type allele observed in the parental fibroblasts (Fig. 7 B).

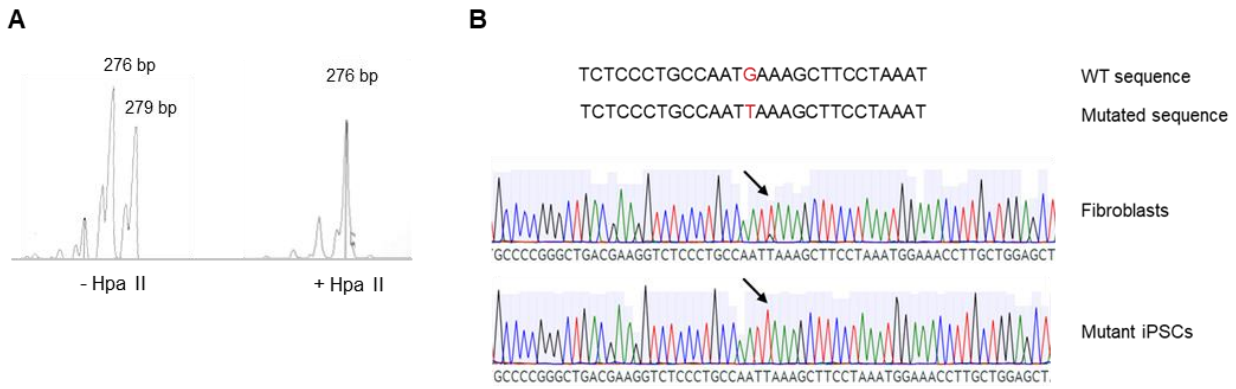

Figure 7

X chromosome inactivation analysis in patient-derived cells. (A) *Analysis by capillary electrophoresis of amplification of the polymorphic CAG repeat within the AR gene from HpaII-digested (+HpaII) and non-digested (-HpaII) DNA in patient-derived fibroblasts. Results show two alleles of different size in the non-digested DNA and a single amplification product after HpaII digestion, consistent with an extremely skewed XCI pattern. The size of the allele is determined by the number of repeats.* ***(B)*** *Sanger sequencing of cDNA from fibroblasts and iPSCs. In the sequencing chromatogram from parental fibroblasts both peaks are present, but at very different height (black arrow). A single peak (T) is present in the sequencing chromatogram from fibroblast-derived iPSCs (black arrow). Wild type and mutated sequences are shown at the top. The c.1090G>T change is outlined in red. The wild type allele carries a G, while the mutant has a T.*

iPSCs can be differentiated into mixed cultures of neurons using an induction protocol for the generation of SNMs

To provide a disease model for realistic representation of the patient and her genetic background, we exploited iPSCs potential to be differentiated *in vitro* into neurons.
We differentiated iPSCs to Neural Precursor (NP) cells modifying a published protocol that involves the formation of EBs and SNMs (80). Briefly, iPSC colonies were cultured on bacterial dishes to form EBs. Then, the EBs were transferred onto Matrigel-coated culture dishes and cultured in the presence of basic FGF (bFGF) and N2 supplements for 10 days. When neural clumps with neural rosettes or neural tube-like morphologies were formed, they were isolated mechanically and cultured in suspension on bacterial dishes in the presence of bFGF and N2 supplements. After approximately 7 days in this culture condition, SNMs were formed (Fig. 8 A).
To differentiate SNMs into neurons, we transferred the SNMs onto Matrigel-coated culture wells in the presence of basic FGF (bFGF) and N2 supplements. A week later, cells displayed neuronal morphologies with processes (Fig. 8 B).

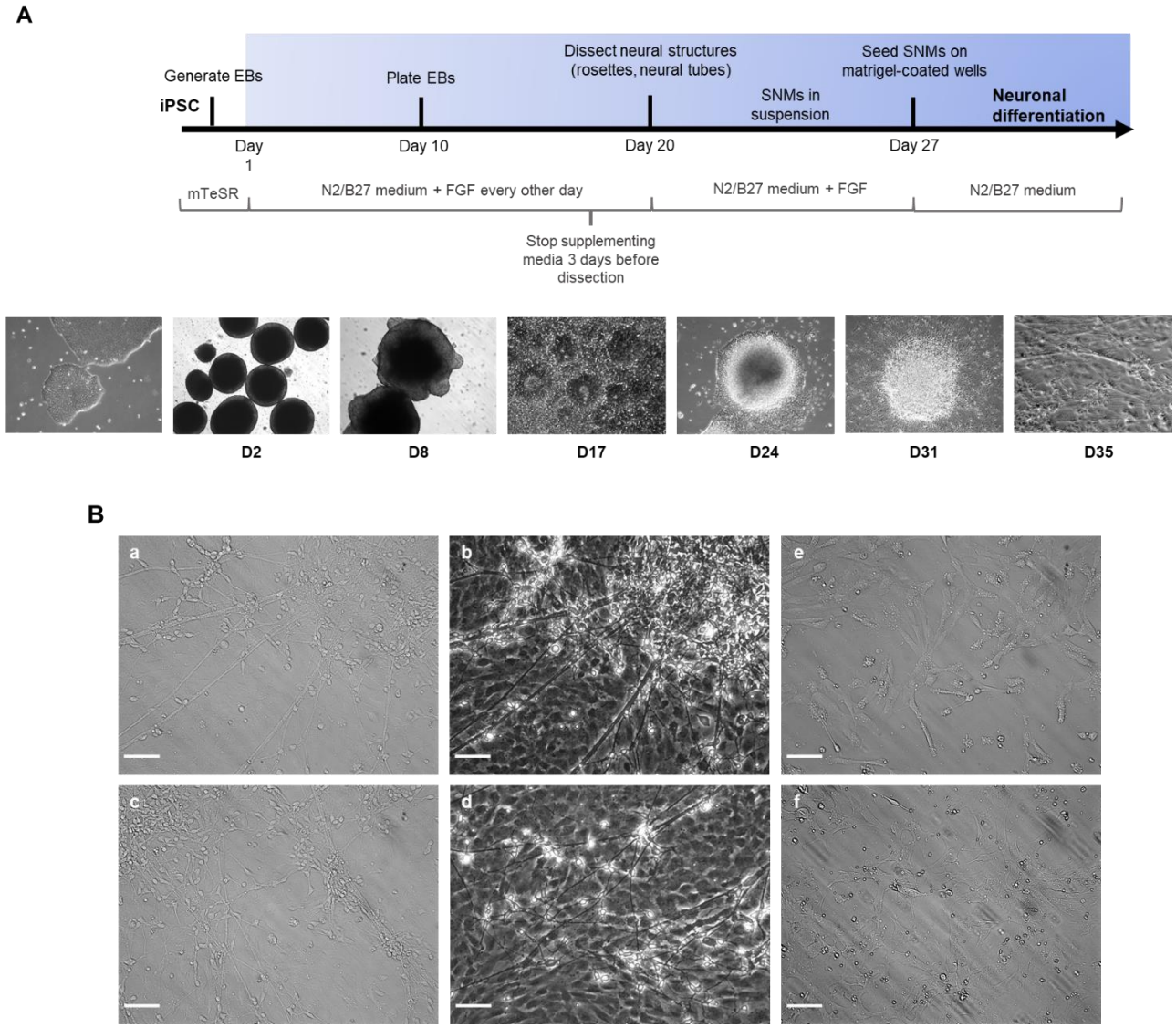

Figure 8

Differentiation of iPSCs into neurons. (A) *Schematic representation of the procedures for the in vitro differentiation of iPSCs: after EBs formation and subsequent selection and expansion of NPs with neural rosettes and neural tube-like structures, SNMs were made by growing the NPs in suspension culture. The SNMs were then seeded and differentiated into neurons. The lower panel shows culture morphology at different time points.* ***(B)*** *Representative brightfield and phase-contrast of neuronal-like (a-d) and glial-like cells (e-f) at d35 of differentiation. Scale bars = 50 µm.*

After culturing cells for 3 weeks more, immunostaining was performed by using antibodies against Microtubule-Associated Protein (MAP2), Glial Fibrillar Acidic Protein (GFAP), and Synapsin 1 (SYN1). MAP2 is a widely used cytoskeletal marker for mature neurons, while GFAP is a marker for radial glia and astroglia. SYN1 is a synaptic marker, and it locates on the cytoplasmic face of the synaptic vesicles. At 8 weeks of differentiation, we observed a mixed population of MAP2-positive mature neurons and GFAP-positive cells. There was no apparent colocalization of the two markers. In addition, MAP2-positive neurons showed expression of the synaptic marker SYN1, indicating their capability to form synapses (Fig. 9).
We thus demonstrated that iPSCs can be used to generate SNMs that can then be differentiated into functional cells after about 28 d of maturation in vitro. Under these conditions, SNMs generate dense neuronal networks, confirming their neurogenic capacity.

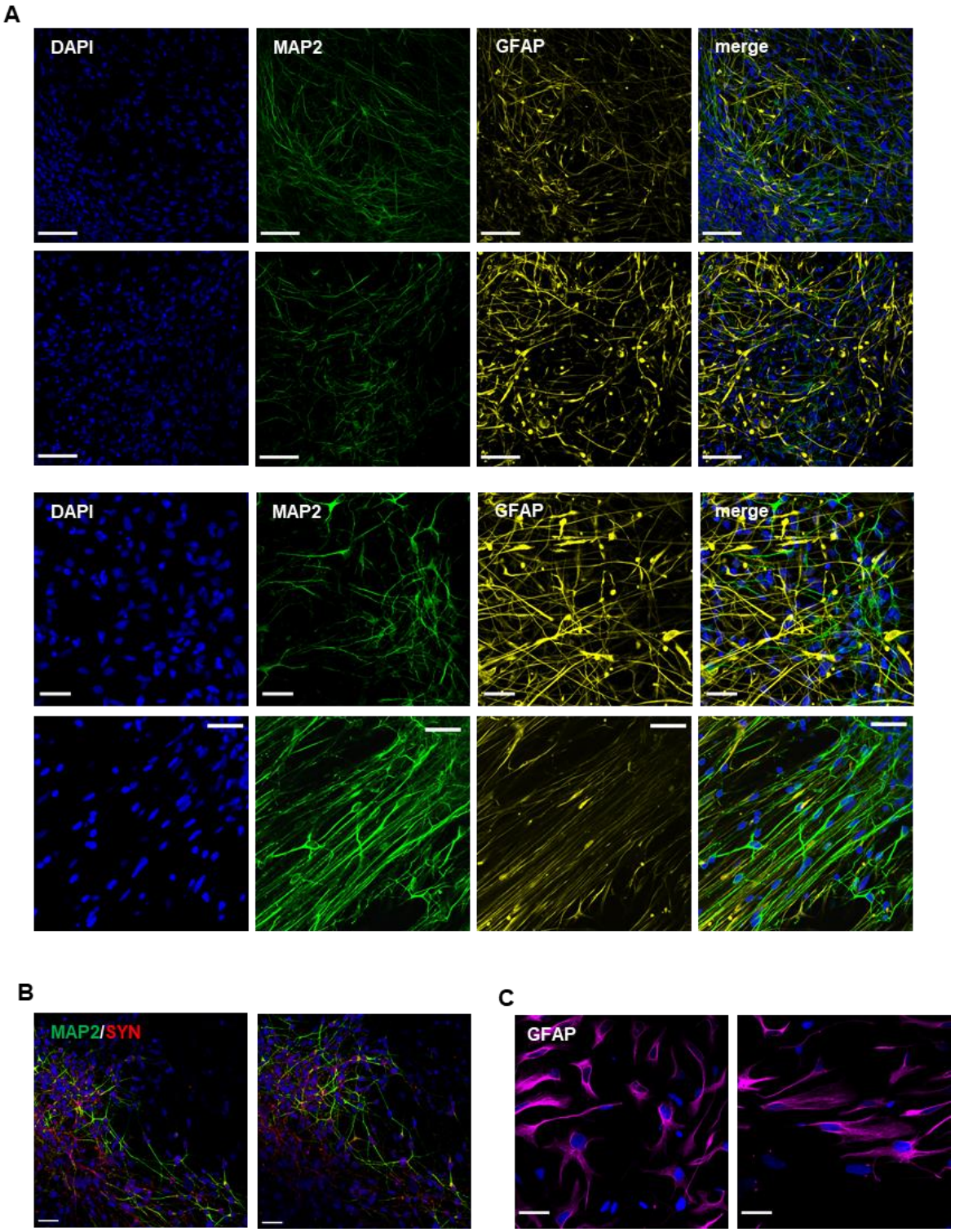

Figure 9

Immunocytochemistry of cultured neurons. (A) *Confocal images of 8-week-old neuronal cultures labelled with MAP2 and GFAP. Cell nuclei were stained with DAPI and are shown in blue. Scale bars = 30 µm (upper panel) and 15 µm (lower panel).* ***(B)*** *Confocal images of 8-week-old neuronal cultures labelled with MAP2 and SYN. Cell nuclei were stained with DAPI and are shown in blue. Scale bars = 30 µm.* ***(C)*** *Images of astrocyte-like cells labelled with GFAP. Cell nuclei were stained with DAPI and are shown in blue. Scale bars = 15 µm.*

X chromosome inactivation in female iPSC lines is preserved upon neural differentiation

We next tested whether the XCI observed in undifferentiated iPSCs is maintained upon induction of differentiation into neural cells. *CDKL5* mRNA analysis by RT-PCR and Sanger sequencing demonstrated that iPSC-derived neural cells exclusively express the mutant allele, indicating that XCI is preserved upon differentiation (Fig. 10).

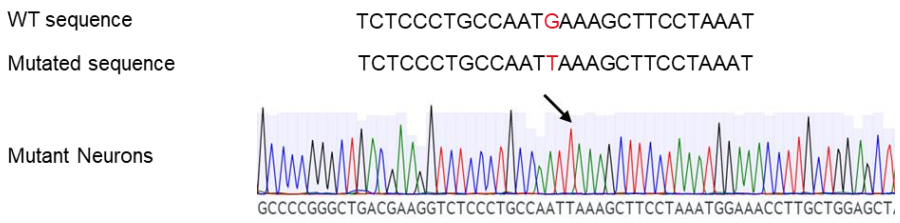

Figure 10

Sanger sequencing of cDNA from mutant neurons. *Wild type and mutated sequences are shown at the top and the 1090G>T change is outlined in red. The wild type allele carries a G, while the mutant has a T. In the sequencing chromatogram a single peak (T) is present (black arrow), indicating exclusive expression of the mutant allele.*

Plasmid-based delivery of CRISPR/Cas9 system results in variable editing efficiency

In this study, we initially performed CRISPR-mediated *CDKL5* editing in cultured fibroblasts using a plasmid-based approach, to evaluate the efficacy of gene correction in a patient-specific cell model. We have previously demonstrated that it is possible to correct mutations in *FOXG1* and *MECP2 in vitro* using a plasmid-based system to deliver CRISPR reagents (86,87).
In light of these encouraging results, we tested co-transfection of two plasmids delivering Cas9 protein and guide RNA to the host cells together with a DNA donor template.
The genomic sequence was analysed to locate PAM sequences in close proximity of the target site. The PAM site is necessary for recognition by the gRNA/Cas9 complex, and it should be located directly downstream of the target sequence in the genomic DNA, on the non-target strand. Based on these criteria, we engineered the pAAV2.1 U6-gRNA-CDKL5 and the pX551 vectors. To improve the detection of transfected cells, we introduced a unique fluorescent fusion protein into the pAAV2.1 U6-gRNA-CDKL5, where EGFP (green) and mCherry (red) fluorescent proteins are used under CMV promoter to enable dual labelling. The target sequence (PAM+gRNA) was engineered into the mCherry-EGFP fusion gene disrupting the open reading frame (ORF) of EGFP gene. Therefore, while mCherry is constitutively expressed in transfected cells, the fluorescence of EGFP is only observed when Cas9 (pX551) is expressed and cleaves the target sequence, restoring EGFP's ORF (Fig. 11).

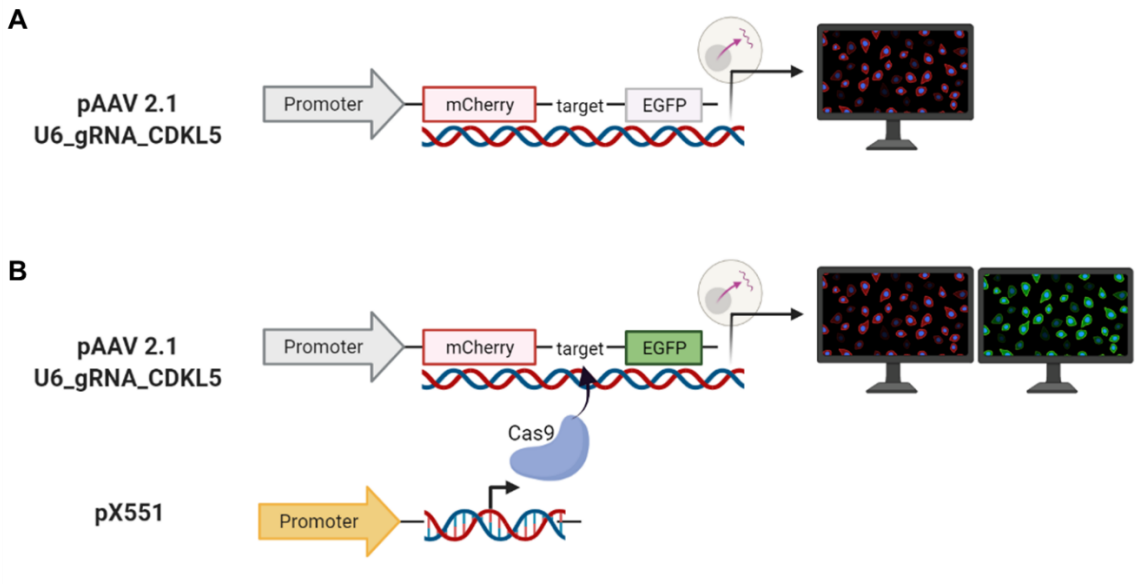

Figure 11

Dual fluorescence reporter for labelling of cells transfected with pAAV2.1 U6-gRNA-CDKL5 and pX551. (A) *Transfection of the pAAV2.1 U6-gRNA-CDKL5 where the EGFP is cloned out of frame results in transient red fluorescent signal.* ***(B)*** *Co-transfection of pAAV2.1 U6-gRNA-CDKL5 and pX551 results in Cas9-mediated EGFP reading frame restoration and emission of red and green fluorescence.*

We first tested various concentrations of plasmid DNA and determined 1:3 as the optimal plasmid ratio between pAAV2.1 U6-gRNA-CDKL5 plasmid and pX551 Cas9 expressing vector. One million cells were transfected with 3 µg of pAAV2.1 U6-gRNA-CDKL5 plasmid and 9 µg of the pX551 Cas9 expressing vector. The pattern of fluorescence was first observed using fluorescence microscopy: mCherry is always expressed in the initial stages after transfection, while EGFP fluorescence was rarely observed earlier than 24 hours post-transfection. The time for plasmid-driven expression and activation of Cas9 nuclease activity explains the absence of green fluorescence during the early stages after transfection. Flow cytometry was used for the precise quantitation of the cells that express the specific fluorescent genes. Transfection efficiency, determined by quantitation of mCherry was 84,2±2,3% (Fig. 12 A). The presence of the EGFP fluorescent protein marker on the pAAV2.1 U6-gRNA-CDKL5 plasmid allowed us to use FACS to enrich the cells that had received and expressed both Cas9 and gRNA. EGFP+ co-transfected cells were quantitated and collected using a FACScan flow cytometer. The average percentage of EGFP+ cells 48 hours after transfection was 3,5±1,5% in three independent experiments (Fig. 12 B).
Following isolation of DNA from EGFP+ cells, we used Next-Generation Sequencing (NGS) to characterize the targeted DNA region and estimate the level of HDR. Although the coverage across the target site was not high, it was possible to analyse the resulting reads against a reference genome (Fig. 12 C). We used Cas-Analyzer, a JavaScript-based implementation for NGS data analysis, that requires uploading raw output data in FASTQ format with gRNA and ssDNA sequence (88). Since cells are heterozygous for the target variant, we calculated HDR efficiency according to the following formula, where “% corrected alleles” is the value estimated from Cas-Analyzer for both treated sample and not treated control:

$$(\%\ \text{corrected alleles in edited cells} - \%\ \text{corrected alleles in negative control}) \times 2$$

We obtained HDR rates ranging from 4 to 66,4% (33,6±31,3%) in three independent experiments. As was expected, NGS data analysis revealed that dsDNA-mediated DSB repair did not only lead to the introduction of the intended base pair change, but also caused NHEJ-mediated insertion/deletion at the site of the DSB (2,8±1,8%, calculated as described above).

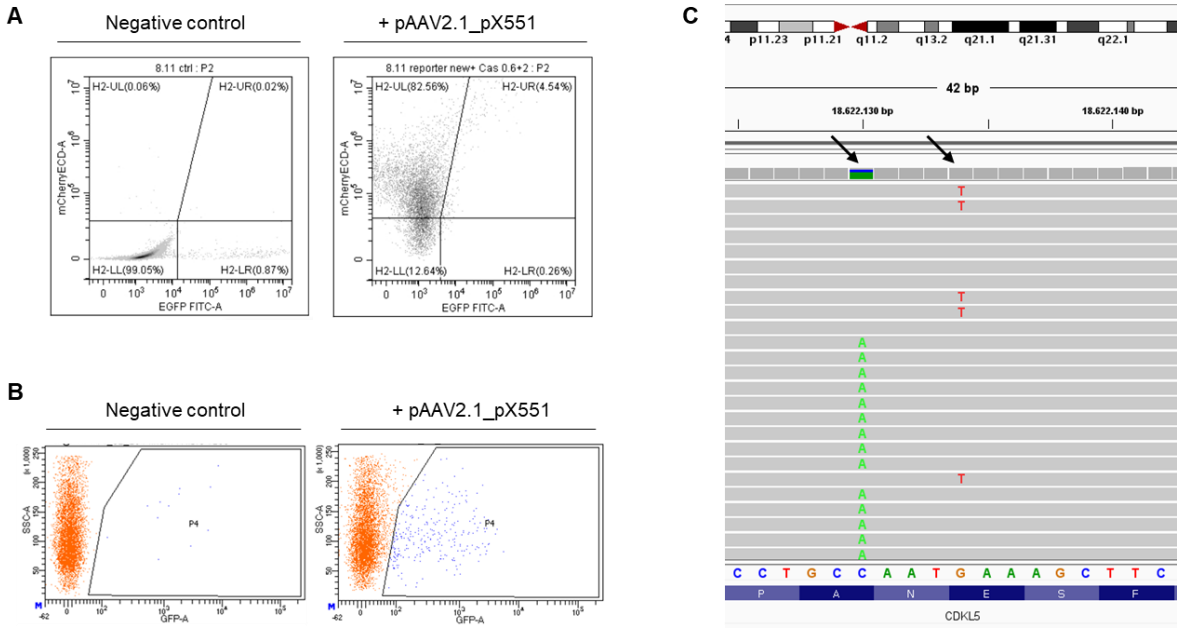

Figure 12

FACS and NGS analysis of fibroblasts transfected with pAAV2.1 U6-gRNA-CDKL5 and pX551. (A) *FACS plot of cells transfected with pAAV2.1 U6-gRNA-CDKL5 and pX551 (on the right) showing representative data from one of two separate experiments. Cells in the upper right quadrant are mCherry/EGFP+. The percentage of cells in this population is indicated. Debris and doublets were gated out of the analysis. Negative transfection control plot is on the left.* ***(B)*** *Sorting by FACS of cells transfected with pAAV2.1 U6-gRNA-CDKL5 and pX551 constructs. The graph shows the events detected by FACS plotted as GFP fluorescence intensity (GFP-A) versus diffracted light intensity (SSC-A). About 100,000 events were recorded and the particles corresponding to those falling into box P4 were collected. Negative transfection control is on the left. The graph shows representative data from one of three separate experiments.* ***(C)*** *Representative image of Integrative Genomics Viewer (IGV) visualization of alignments of the targeted NGS sequencing results showing the insertion of the silent mutation outlined in green (black arrow on the left). On the right, the mutation outlined in red is marked with a black arrow*

.

Optimized CRISPR/Cas9 design for correcting the *CDKL5* E364X mutation

In light of the extremely variable editing efficiency achieved in our initial experiment, we decided to test additional gRNAs. To improve the *in vitro* efficiency of CRISPR/Cas9-mediated correction and expedite the selection process, we also elected to directly deliver Cas9 protein and a synthetic gRNA as a RNP complex, rather than as a plasmid.

Based on previously descried criteria (see Plasmid-based delivery of CRISPR/Cas9 system results in variable editing efficiency), we identified three candidate gRNAs (Table 3).

To confirm that the gRNAs could direct cutting at the target sequence and to select the most effective one, we performed an *in vitro* digestion assay with a PCR amplicon amplified from genomic DNA that contained the gRNA target sequence, together with Cas9 nuclease and gRNA. In the presence of the gRNAs, Cas9 nuclease cut the amplicon into 325 and 256 bp fragments, consistent with the predicted sizes of the fragments. Integrated density, calculated as the sum of the values of the pixels in the image, was measured with image J software to quantify the intensities of the bands and determine the DNA cleavage efficiency. The gRNA1 (lane 2; RNP1) exhibited the higher cleavage efficiency (87%). As to gRNA2 and gRNA3 (lanes 3 and 4; RNP2 and RNP3), cleavage efficiency was in the range of 65-80% (Fig. 13 A).

These results were overall confirmed by the T7 endonuclease I mismatch detection assay, that is commonly employed to evaluate the gene editing efficiency of CRISPR/Cas9 reagents at a given guide RNA target site. The T7 endonuclease I, in fact, recognizes and cleaves structural deformities in DNA heteroduplexes and allows for a rapid estimation of gene editing percentage in mixed populations of edited cells. Briefly, either RNP1 (gRNA1-Cas9), RNP2 (gRNA2-Cas9) or RNP3 (gRNA3-Cas9) were assembled and separately delivered to the mutant iPSCs. PCR amplification with primers around the editing site generates mutant and edited PCR products. Denaturing and reannealing of these products generates mismatches that are cleaved by the T7EI nuclease. Running these PCR products on a gel resolves full length DNA and cleavage products. Where present, cleaved fragments of the expected sizes indicate that the gRNA successfully cleaved the target region generating indels. The gRNA1 (lane 2; RNP1) was confirmed as the most efficient compared to gRNA2 (lane 3; RNP2) with 48% and 45% cleavage efficiency, respectively, while there was no detectable cleavage using gRNA3 (lane 4), as displayed in Figure 13 B. Consistent with these findings, the gRNA1 was selected for the editing procedure.

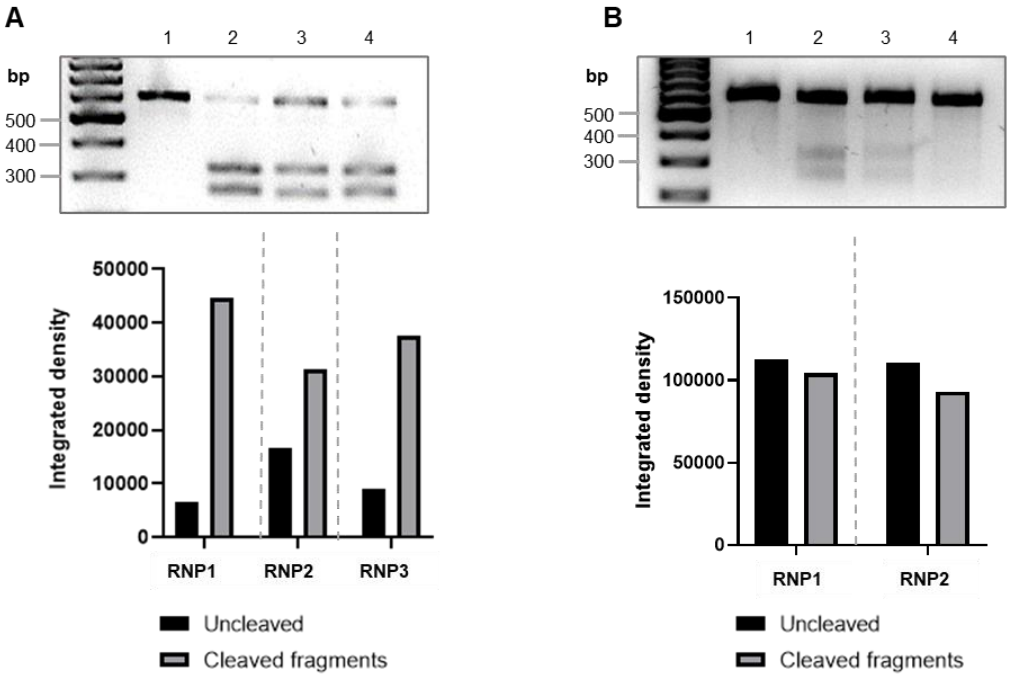

Figure 13

Cleavage efficiency of the selected gRNAs. (A) *In vitro dsDNA cleavage by SpCas9 of gRNA1, gRNA2 and gRNA3 (lane 2, lane 3, and lane 4, respectively). A negative control that lacked gRNA was included for comparison (lane 1). Cleavage efficiency was assessed by agarose gel electrophoresis (upper panel) and measured using densitometry (lower panel).* ***(B)*** *Mismatch cleavage with T7 Endonuclease I in iPSCs transfected by nucleofection of either RNP1, RNP2 or RNP3 (lanes 2, 3 and 4). A negative control of not transfected iPSCs was used as control (lane 1). Cleavage at heteroduplex mismatch sites was assessed by agarose gel electrophoresis (upper panel) and measured using densitometry (lower panel).* ***(A-B)*** *For each lane, the band at the top represents the uncleaved DNA (582 bp) and the bands at the bottom represent the digested fragments (325 bp and 256 bp).*

Nucleofection of RNPs leads to efficient allele-specific editing in iPSCs

Following validation of the activity of gRNA in iPSCs, we designed a repair template in the form of a ssDNA for the correction of the mutation via HDR.
The ssDNA designed would convert the mutant T into the wild-type G to correct the c.1090G>T variant. Moreover, a synonymous nucleotide change (C>A) in the PAM was created to disrupt the CRISPR recognition and cut site and avoid re-cleavage of the target DNA by Cas9 after HDR repair. The PAM silent mutation destroyed a *BsaI* restriction enzyme site; thus, the PAM silent mutation could also be used to facilitate genotyping of HDR events.
The iPSC line clone U generated from patient's fibroblasts was transfected with the RNP complex and the ssDNA and then expanded for screening of HDR events. To get a general idea that some editing occurred, we first screened the mixed population by PCR amplification followed by restriction enzyme digestion. *BsaI* digestion of the amplicon showed that cells underwent Cas9-induced DSB with loss of the restriction site (Fig. 14 A). The analysis of the restriction enzyme digestion profiles allowed us to determine that the digestion ratio (calculated as the ratio of cleavage products and uncleaved DNA) was reduced in cells transfected with RNP1 compared with negative transfection control, showing that editing events have occurred in the polyclonal cell population (Fig. 14 B).

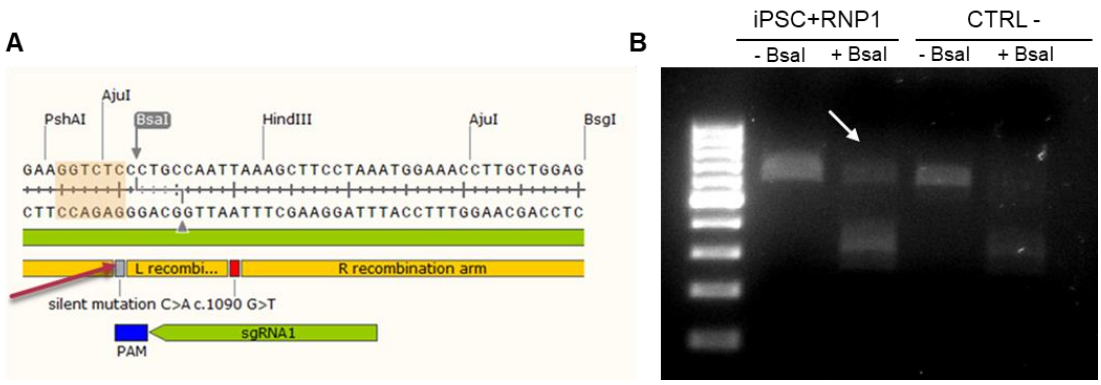

Figure 14

Restriction digest screening of the mixed population. (A) *Schematic representation of the abolition of the BsaI recognition sequence 5'-GGTCTC(N1)/(N5)-3' (outlined in orange) resulting from the use of the HDR ssDNA template (yellow) with the silent nucleotide change at the PAM site (grey) indicated by a red arrow.* ***(B)*** *Digestion profiles of the mixed population of cells transfected with RNP1 (on the left) and negative transfection control (on the right). Uncleaved DNA band is present in the transfected sample (white arrow) but absent in the negative transfection control. Negative digestion reaction without enzyme were included and loaded at the left of each sample. Marker: 100bp DNA Ladder (Invitrogen).*

We then proceeded with the isolation of clonal cell lines from the mixed population of edited cells. A highly diluted cell suspension was obtained, and single cell-derived clones were isolated and further expanded. We investigated HDR events by Sanger sequencing, both before and after subcloning of the PCR products. First, genomic DNA from the modified region was amplified from individual subclones and screened by both *BsaI* digestion and Sanger sequencing to reveal the genotype. It was possible to identify two CRISPR/Cas9-modified clones that were positive for the targeted modification, as determined by the correction of the heterozygous mutation and the presence of the synonymous change in the targeted allele (Fig. 15 A). However, we observed that not HDR-mediated modifications (indels) account for the destruction of the *Bsa*I recognition site and the decrease of *Bsa*I digestion in five more screened clones. Next, gene-correction in one clone was validated by TA cloning to sequence individual alleles found within the clone. TA cloning is one of the simplest and most efficient methods for the cloning of PCR products. HF Phusion polymerase-amplified PCR products were directly inserted into a plasmid for transformation into the competent cell line. Ten positive colonies were selected and subsequently analysed for the presence of the expected

modification. Sequencing analysis of the insert showed that the system was able to recognize and induce specific cutting of the target allele containing the mutation while preserving the wild type allele. Moreover, sequencing analysis of ~1kb region around the CRISPR cutting site demonstrate that no further cutting occurred, and that the DNA sequence remained intact without frameshift or other mutations (Fig. 15 B).

In conclusion, we were able to generate two isogenic genetically corrected iPSC clones using the CRISPR/Cas9 technology, where the mutated triplet TAA (stop codon) was corrected to the wild-type triplet GAA (Glutamate) through direct delivery of RNP together with a ssDNA as a homologous template. It is important to underline that, since the isogenic cell line was obtained by means of direct editing of cells derived from the affected individual, we have eliminated interindividual genomic heterogeneity resulting from the genetic background.

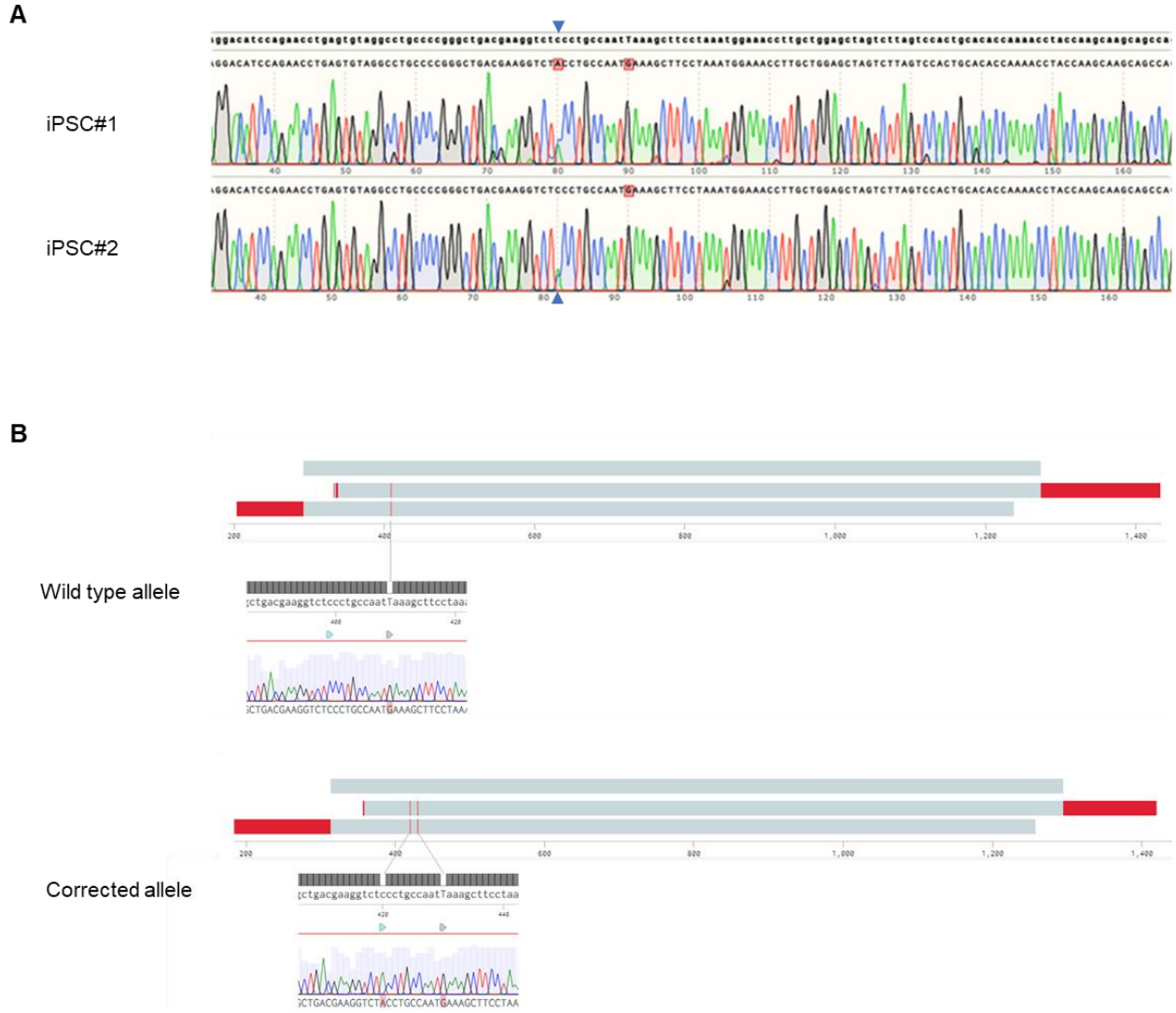

Figure 15

Genetic validation of the generated corrected lines. (A) *Sanger sequencing data from selected targeted iPSC clones indicated that gene correction was achieved. A double peak (C/A) is present at the location of the silent mutation in the chromatograms, as the change is heterozygous (blue pointing triangles). A single peak (G) is present at the site of the mutation showing that the mutant allele (T) has been replaced by the wild type allele (G). Sequences are aligned to the reference sequence from the patient, outlined in black letters at the top of the panel. Changes in the sequences are marked by a red box in the text sequence along the top.* ***(B)*** *Sequencing of DNA fragments amplified from iPSC clone (iPSC#2) after TA cloning shows either the wild type (upper lane) or the gene-corrected alleles (lower lane). Location of the silent nucleotide change and mutation site are indicated by blue and grey right-pointing arrowheads, respectively. The grey bar represents the insert cloned into the vector.*

MAP2 expression is different in mutant and isogenic genetically corrected neurons

Undifferentiated mutant and gene-corrected iPSC clones did not show any major difference. We then generated a neuronal cell model by neural induction of mutant and gene-corrected iPSCs, where we could demonstrate the functional consequences of the edit in the disease-specific cell type. Immunostaining with anti-MAP2 and anti-GFAP antibodies confirmed the presence of MAP2-positive mature neurons and GFAP-positive cells (Fig. 16 A). Interestingly, quantitative analysis of eight randomly chosen stacks highlighted a statistically significant difference in immunocytochemical expression of MAP2 in mutant and corrected samples, with mutant cells showing increased fluorescence intensity of MAP2 compared to corrected cells. We observed robust expression of *GFAP* with no statistically significant differences between the two samples (Fig. 16 B).
We also tested the expression of *MAP2* and *GFAP* genes in our mutant and corrected neuronal cultures by RT-qPCR. The expression analysis highlighted a statistically significant difference in *MAP2* and to a lesser extent *GFAP* mRNA expression. In particular, the mutant cells showed reduced expression of *MAP2* and *GFAP* compared with the corrected ones (Fig. 16 C).

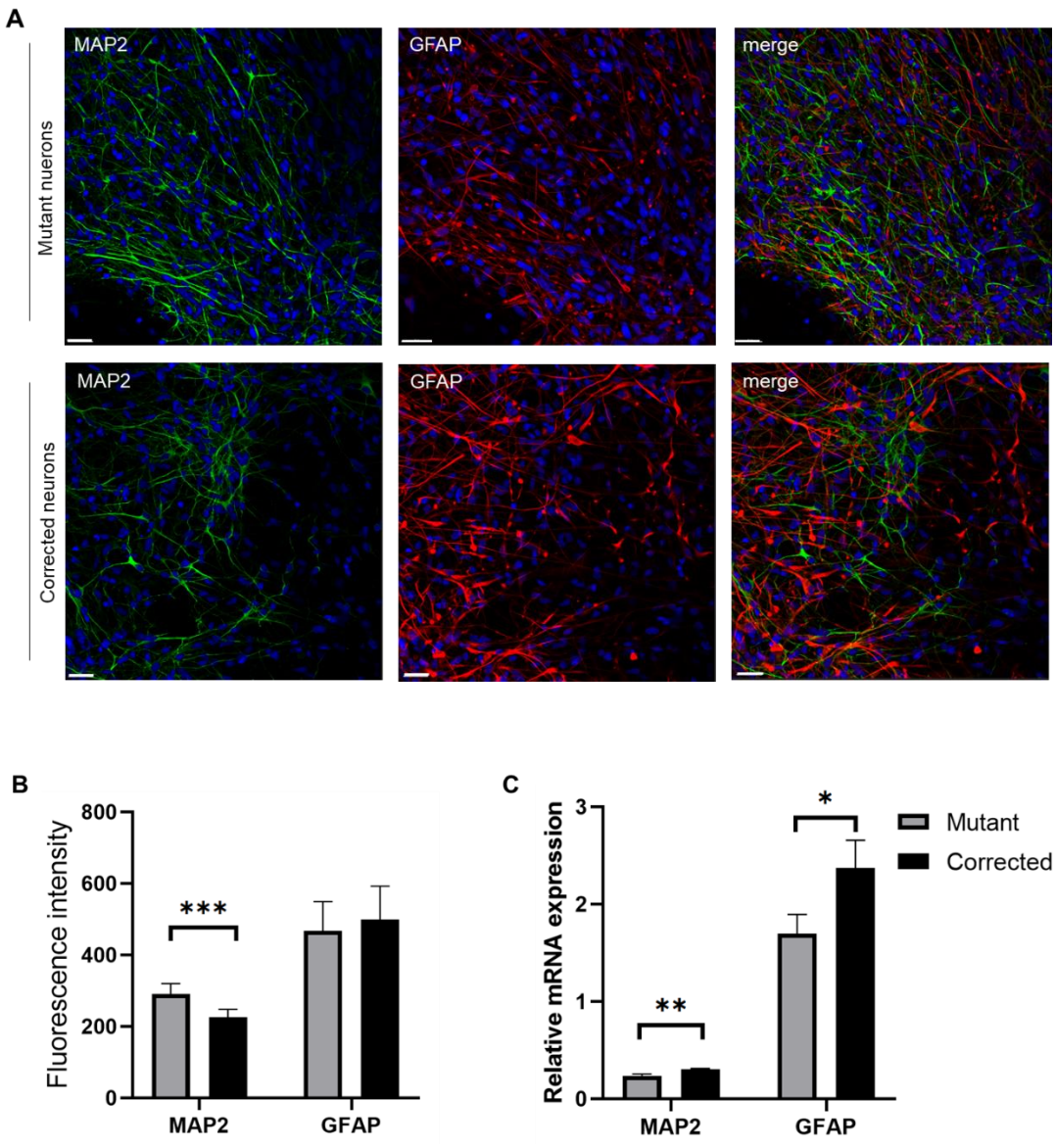

Figure 16

Expression of neural and glial markers in neuronal cell cultures. (A) *Representative confocal images of 8-week-old mutant (upper panel) and corrected neural cells (lower panel) labelled with MAP2 and GFAP. Cell nuclei were stained with DAPI and are shown in blue. Scale bars = 30 µm.* ***(B)*** *Graphic illustration showing quantitation of MAP2 and GFAP fluorescence intensity expressed as the ratio of intensity sum and surface volume. Groups were compared using unpaired t test; *** $p \leq 0.001$ (n=8).* ***(C)*** *Relative expression of MAP2 and GFAP genes in both mutant and corrected groups were normalised to the GADPH gene as a reference gene. Each histogram represents the mean ± SD of three replicates. Statistically significant differences are marked as * $p \leq 0.05$ and ** $p \leq 0.01$.*

CRISPR/Cas9-mediated gene editing restores CDKL5 expression in iPSC-derived neurons

We decided to assess CDKL5 protein expression using western blot. The E364X mutation creates a premature termination codon that is predicted to generate a truncated CDKL5 protein lacking a large part of the C-terminal region. Accordingly, western blot analysis confirmed the absence of the full-length protein in the mutant iPSCs and neurons. CDKL5 protein was, however, expressed in gene-corrected neurons (Fig. 17). It wasn't possible to confirm or exclude the presence of truncated proteins of smaller size using commercially available antibodies, due to either unfit epitope location (C-terminal compared to the mutation site) or optimization failure. Therefore, at the moment, it is unknown whether the mutation results in the presence of truncated non-functional CDKL5 protein or in its complete absence.

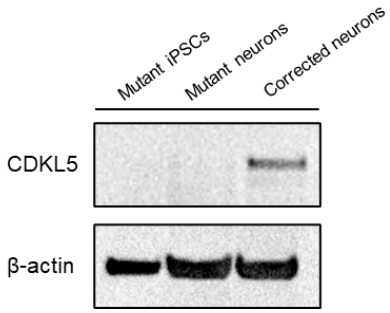

Figure 17

CDKL5 expression in isogenic genetically corrected neurons. *Western blot analysis of CDKL5 show the presence of full-length CDKL5 protein in whole neural cell lysates isolated from gene-corrected neurons but not in mutant iPSCs and neurons (upper panel). β-actin was used as loading control (lower panel).*

CDKL5 mRNA expression is reduced in CDD mutant neurons compared to isogenic control

We further evaluated the expression of *CDKL5* at the mRNA level in mutant and CRISPR/Cas9-corrected iPSC-derived neural cells originating from the same individual. In order to compare *CDKL5* mutant and corrected transcript expression, we assessed *CDKL5* transcript by quantitative RT-PCR. As shown in Figure 18 A, the mutant neurons carrying c.1090G>T show expression levels that were significantly lower than in isogenic gene-corrected neurons.
We further characterized the neuronal population by investigating the expression of *NMDAR1* (N-methyl-D-aspartate receptor 1), *NMDAR2* (N-methyl-D-aspartate receptor 2), *GAD1 (*Glutamic acid decarboxylase 1), and *GAD2* (Glutamic acid decarboxylase 2) genes in mature cultures by quantitative RT-PCR. We found very different expression levels between the two classes of markers. Based on RT-qPCR, neural induction seems to have generated a population enriched of GABAergic neurons, as shown by the prevalent expression of *GAD1/2* (Fig. 18 B). We observed a statistically significant difference in *GAD1*, *GAD2* and *NMDAR1* mRNA expression between the mutant neurons and the corrected isogenic ones. In particular, the corrected cells showed higher expression of *GAD1* and to a lesser extent *GAD2* and *NMDAR1* compared with the mutant cells. Expression of *NMDAR2* was similar in mutant and corrected neurons (Fig. 18 B).

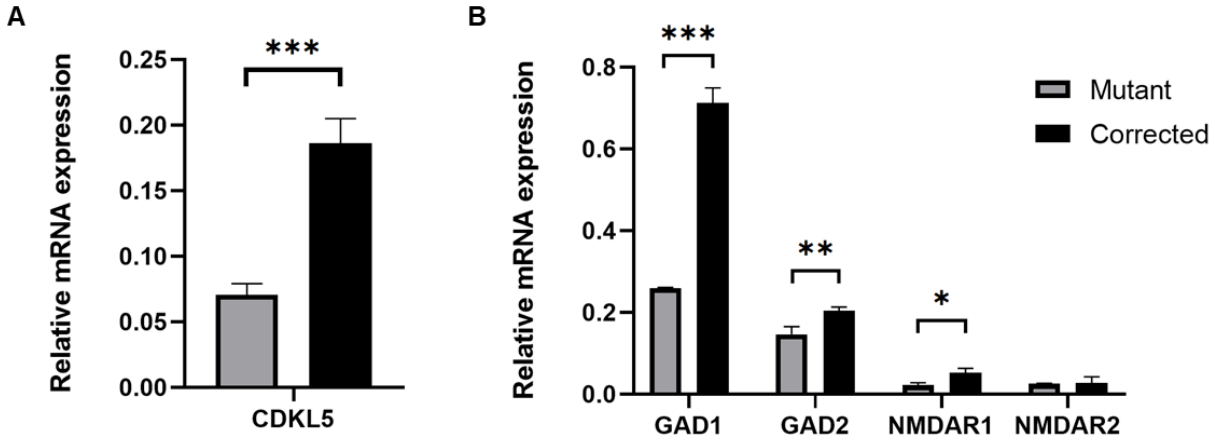

Figure 18

RT-qPCR results in neuronal cells. *Graphic illustration showing the relative level of expression of CDKL5* ***(A)*** *and GAD1, GAD2, NMDAR1 NMDAR2* ***(B)*** *in mutant and genetically corrected neural cells. Expression of genes in both mutant and corrected groups were normalised to the GADPH gene as a reference gene. Each histogram represents the mean ± SD (n = 3). Statistically significant differences are marked as ***p ≤ 0.001.*

Discussion

Mutations in the X-linked *CDKL5* gene cause CDD, a devastating condition affecting kids at a very early stage of life. Individuals with CDD have severe epileptic encephalopathy, global developmental delay and intellectual disability that greatly impact patients' quality of life (5,89,90). However, therapeutic possibilities are still limited to the control of secondary symptoms and no targeted therapy addressing the primary pathology of these patients is available (13,15).Taken together, these considerations highlight the importance of the development of novel effective therapies to treat CDD.
In this study, we demonstrate the feasibility of using CRISPR/Cas9-mediated genome editing to correct a disease-causing heterozygous mutation in *CDKL5 in vitro*. To the best of our knowledge, this is the first time DSB-mediated HDR using the CRISPR/Cas9 system was used to correct disease-causing mutations in *CDKL5*.

Gene therapies are the only form of causal treatment of disorders caused by *CDKL5* mutations. Among them, CRISPR/Cas9 genome editing technique has the advantage of using a single non-sequence specific protein combined with a small guiding RNA molecule to enable modifications of genes with high efficiency and accuracy. It also represents the safest approach for the targeted modification of genes whose expression is tightly regulated.
The fundamental roles exerted by the CDKL5 protein in the brain (i.e.: neuronal migration, axonal outgrowth, dendritic morphogenesis and synapse formation) and the spatiotemporal regulation of *CDKL5* expression (8,22), indicate that *CDKL5* levels are strictly modulated. Accordingly, although the CDKL5 disorder is generally associated with loss of function mutations, patients carrying *CDKL5* duplications have recently been reported (91). The use of gene-augmentative therapy through delivery of an intact version of the missing gene, even when provided with all necessary regulatory sequences, would likely not reproduce the subtle regulation of *CDKL5*. On the contrary, genome editing manipulates the natural locus by introducing targeted genomic sequence changes without disrupting endogenous controls.

Approaches to CNS research have always been hindered by difficulties in procuring the cell type primarily affected by the pathology, since brain tissue from patients is obviously not available in humans. On the other hand, post-mortem tissues may originate from individuals at late stages of the disorder and result in an expression profile that may reflect the pathogenesis of concurrent diseases. In this context, iPSCs provide a source of patient-derived cells and a means of creating a human model of CNS disorders. iPSCs are stem cells that have been reprogrammed from adult somatic cells into a pluripotent state and they can give rise to any cell type of the body. Neuronal cultures may be differentiated from human iPSCs, providing a human model that would create a realistic representation of the disease. An attractive application of genome manipulation in human pluripotent stem cells derived from an affected individual is that it allows the generation of cells that have undergone editing events in order to correct the mutation. The resulting pairs of iPSC lines are isogenic, meaning that they are genetically identical (also with respect to the XaXi status), except for the disease-relevant mutation. Parallel differentiation of such isogenic sets of cells into disease-relevant cells and tissues can be used to directly assess the contribution of a mutation to cellular pathology or, as in the case of CRISPR-based editing validation, to demonstrate the functional consequences of the edit in the affected cell type (92–95).

The *CDKL5* gene is found on the X chromosome that is subject to random inactivation in females, to allow gene dosage-compensation between males and females. In female somatic cells one of the two X chromosomes is silenced early during development (96) in a process that typically exhibits a random pattern. Hence, patients with heterozygous mutations display a mosaic distribution of somatic cells expressing either the wild-type or the mutant *CDKL5* allele in their tissues. On the other hand, XCI status in human iPSCs is controversial and it is unclear whether reprogramming of female human cells reactivates the inactive X chromosome (Xi)(97,98).

In this study, we have investigated the X inactivation pattern in DNA from fibroblasts of a CDD female patient with a de novo heterozygous mutation in *CDKL5* creating a premature stop termination. Analysis of the polymorphic CAG trinucleotide repeat of the *AR* gene showed a skewed X-inactivation pattern with a marked deviation from a 50:50 ratio, where each X chromosome is active in an equal number of cells. *CDKL5* cDNA sequence analysis demonstrated that the mutant allele was the one that was preferentially expressed, whereas the normal X chromosome was preferentially inactive. These results confirmed that *CDKL5* is subject to X-inactivation in female somatic cells.
To address the XCI status upon cell reprogramming, we then investigated whether iPSCs obtained by reprogramming of patient's fibroblasts carried an Xi. The iPSCs clones examined preserved XCI, with one of the two X chromosomes exclusively being inactive. Not entirely unexpectedly, all tested iPSC clones exclusively expressed the mutant allele, carrying the wild-type allele on the inactive X chromosome, consistent with the skewing pattern observed in parental fibroblasts. Our data thus confirm that iPSCs derived from female fibroblasts maintain the XCI upon reprogramming of somatic cells. Furthermore, the observation that each iPSC clone only expressed one allele confirms the clonality of the reprogramming process. Interestingly, we show that X chromosome inactivation is maintained upon neural differentiation of iPSCs, consistent with some reports in research modelling of Rett syndrome in human hiPSCs corroborating the hypothesis that the inactivation status of the somatic cell is maintained during reprogramming and differentiation (97,99), although the relevant literature is overall contradictory and lacks of consistency (98,100)
These findings could have critical implications for X-linked disease modelling. In fact, unpredictable patterns of XCI in the presence of heterozygous mutations could compromise the analysis of *CDKL5* gene expression profiles as well as that of the downstream functional pathways. On the contrary, in cells exclusively expressing the *CDKL5* mutant allele, we expect that effects on gene expression profiles and downstream pathways would be highlighted (84), making it possible to effectively compare them to cells expressing wild-type *CDKL5*, thus eliminating variations resulting from the genetic background.

The goal of this study was to develop an efficient CRISPR/Cas9-based genome editing strategy that would allow reliable correction of a *CDKL5* heterozygous mutation in patient-derived cells, as proof of concept to further extend the scope to other pathogenic variants.
We previously reported encouraging results achieved using an identical genome-editing strategy for *FOXG1* and *MECP2* genes with a plasmid-based system (86,87). Relying on these previous results, we developed an analogous system for co-transfection of patient-derived fibroblasts with plasmids expressing Cas9 protein, guide RNA, DNA donor template and a fluorescent reporter to allow detection of co-transfected cells. Specifically, we have designed a fluorescent mCherry-EGFP fusion protein that allows for selection and quantitation of positive cells using flow cytometry. Briefly, the target sequence (PAM+gRNA) was engineered into the mCherry-EGFP fusion gene disrupting the open reading frame (ORF) of *EGFP* gene. Therefore, while mCherry is constitutively expressed in transfected cells, the fluorescence of EGFP is only observed when Cas9 is expressed and cleaves the target sequence, resulting in EGFP reading frame restoration. It should be noted, however, that this is not a 100% accurate system as Cas9-induced indels at the target site are not predictable and might still lead to frameshift of the ORF in a number of cases, resulting in ultimate underestimation of Cas9 activation. This could partly explain why, despite the high transfection rates for mCherry (84,2±2,3%), only 3,5±1,5% of cells were positive for EGFP.
We positively selected EGFP-expressing cells using a FACS approach, thereby enriching the targeted population and avoiding mixed cell populations. HDR efficiency fluctuated between 4 and 66,4% (33,6±31,3%) in the FACS-sorted cells. It is widely known that each step, from the introduction into the cells to the genome editing occurrence, represents a challenge in this system and plasmid-based delivery can result in variable editing efficiencies because of the uncontrollability of gRNA and Cas9 enzyme expression levels. Many factors contribute to transfection success, and most of them are depending on the host cells themselves and are poorly understood and controlled. Variable factors, such as cell cycle progression, circadian rhythm of gene expression activity, promoter activity, and general activity in a given cell type can affect protein expression, altering specificity and kinetics

of gene editing (101), or even inhibit a cell from actually expressing the transfected protein (102). Furthermore, it should be noted that in many cell types, NHEJ is the main pathway of repair, while HDR-mediated precise genome editing mainly happens in the S- or G2- phase of the cell cycle (103). Notably, the DSB repair pathway choices were found to be different in species with distinct genetic backgrounds, and even in cell types of a single species (104). This can affect experimental reproducibility accounting for inter-experimental differences in editing efficiency.
Given the reasonably consistent editing efficiencies reported in our previous works where an analogous methodology was used (86,87), the inter-experimental variability in editing efficiency observed here is probably ascribed to host cell line-dependent factors and denotes a need for protocols to be adjusted for each cell line of interest.

In light of the high variability of editing efficiency, we decided to test additional guides. To expedite the selection process, we replaced the plasmid-based system with a protein-based RNP delivery system, that would guarantee a much more rapid action and great stability, also alleviating difficulties with protein expression that can occur after plasmid or mRNA delivery (76). Moreover, we reckoned it would be more convenient to test the system in human pluripotent stem cells rather than fibroblasts. This iPSC/RNP strategy, in fact, would allow us to subclone cells that have undergone editing events, thus generating an isogenic iPSC line that would differ from the original one for the disease-relevant mutation alone. Parallel differentiation of such isogenic sets of cells into neural cells can be used to directly assess the functional consequences of the edit in the affected cell type.
This strategy, however, comes with some risks. iPSC reprogramming, in fact, can cause genetic instability, as it was our case. The iPSC line used in the study, in fact, was found carry an extra copy of chromosome 8. Due to post thawing viability issues, it was not possible to check whether karyotype anomalies were already present at early passages. However, the non-mosaic pattern of the trisomy suggests that the prolonged culturing due to the extremely low rate of survival after cryopreservation led to the arising of abnormal cells. Notwithstanding that maintenance of a stable karyotype is required for clinical use of pluripotent stem cell lines, since our purpose was to create an isogenic cell-line model to study the effects of a mutated X-linked gene at the RNA and the protein level, and compelled by the lack of other stable clones, we decided to proceed with this iPSC clone for the editing procedure.

We initially designed three gRNAs. All three of them showed to be highly efficient by in vitro digestion assay, with cleavage efficiency from 65 to 87%.
In addition, the cleavage activity of the gRNAs in the present study was tested using the T7E1 assay. Consistent with what we observed in the in vitro cleavage assay, gRNA1 was confirmed as the most efficient at producing indels compared to gRNA2, while there was no detectable Cas9-induced DSB using gRNA3. The gRNA1 was thereby selected for the editing procedure.
We designed a ssDNA with a silent mutation in the PAM sequence that destroyed a *BsaI* restriction enzyme site to facilitate genotyping of HDR events. After sequencing analysis of several clonal cell lines isolated from the mixed population of edited cells, we observed that either HDR-mediated repair or NHEJ-generated indels had disrupted the *Bsa*I recognition site. Nonetheless, after validation of the edit by TA cloning, it was possible to identify at least one clone positive for the targeted modification, as determined by the correction of the c.1090G>T mutation and the presence of the PAM silent mutation in one allele. These results show that our editing system is able to recognize and induce specific cutting of the target allele containing the mutation. Moreover, our sequencing analysis of the region around the CRISPR cutting site did not detect any DSB-induced mutations. However, it is possible that there were some undesired CRISPR-generated mutations that were not detected in the present study.
In conclusion, we were able to generate a gene-corrected iPSC clone using the CRISPR/Cas9 technology, where the mutated triplet TAA (stop codon) was corrected to the wild-type triplet GAA (Glutamate) through direct delivery of RNP together with a ssDNA as a homologous template.

It is tempting to speculate that our system selectively targets the mutated X-linked allele, while preserving the wild type allele. However, it should be noted that iPSCs used in this study were carrying the wild-type allele on the inactive X chromosome. Although it is still a subject for debate, literature generally reports that Cas9 activity is inhibited by heterochromatin (105–107). On the other hand, there are studies showing that the enzymatic activity of SpCas9 is not affected by the DNA methylation (108,109). Therefore, whether allele-specific editing results from the specificity of our targeting system for the mutation or rather the limited accessibility of the inactive X chromosome by Cas9 nuclease remains to be clarified.

In order to measure the impact of CRISPR/Cas9 genome editing in the disease-relevant cells, we differentiated gene-corrected and mutant iPSCs into neural cells, adapting a previously published protocol for the generation of dopaminergic neurons from human embryonic stem cells (hESCs)(80). We showed that the iPSCs can be differentiated into neurons and that the differentiation process follows the stages observed in hESCs. We demonstrated that cells require about 60 d differentiation to mature into neurons. Cells in mature culture displayed neuronal morphologies confirmed by expression of pan-neuronal marker MAP2. In addition, expression of the synaptic marker SYN1 demonstrates their capability to form synapses. The very dense network of cells did not allow us to directly estimate the relative percentages of MAP2-positive neurons in the two populations. However, although an accurate quantitation could not be performed, a comparative analysis of MAP2 after random locations acquisition showed a significant difference in fluorescence intensity between the mutant and isogenic cells. In particular, mutant neuronal cells seem to have a higher expression of MAP2 compared with the gene-corrected cells. In contrast with our expectations, RT-qPCR analysis of *MAP2* mRNA expression showed a reverse trend compared with the evidence provided by immunocytochemistry, with reduced expression in the mutant sample compared to the isogenic one. These conflicting results are difficult to interpret and would require a deeper characterization. Although reduction in the levels of MAP2 has been associated to dendritic alterations in RTT patients (110–112), we still need to understand in more detail how precisely CDKL5 regulates microtubule dynamics during dendritic arborisation. Microtubule-associated proteins, such as MAP1S and MAP2, are found to be deregulated in CDD and functionally linked to CDKL5 (113,114). However, even if growing evidence suggests that there is a link between CDKL5, microtubules dynamics, and microtubule-associated proteins, the functional consequences of this interaction are still unknown.

We observed that the neuronal cultures contained heterogeneous cell populations, with many non-neuronal cells that were negative for MAP2 and positive for GFAP staining. GFAP is used as a specific marker for the identification of astrocytes, that are the major glial cell of the CNS. However, it has been reported that proteins having similar molecular weights, isoelectric points, and immunoreactivity with GFAP can be found in cells of neural crest and ectodermal origin and that it constitutes a major portion of the myelin-free axon fraction (115). In agreement with the immunocytochemical findings, we could observe robust expression of *GFAP* mRNA by RT-qPCR. Even if a percentage of non-neuronal cells is expected, this observation points out the need for improved differentiation and enrichment of neuronal precursors in order to generate highly pure populations of neural cells.
We further characterized the neuronal population by investigating the expression of neuronal markers in mature cultures by quantitative RT-PCR. We compared NMDA receptor subunits and glutamic acid decarboxylase expression and found very different expression levels between them. Although they can also be expressed in interneurons, playing a role in the regulation of GABAergic transmission in mammals (116,117), NMDA receptors are preferentially expressed by pyramidal neurons, and therefore primarily regarded as excitatory neuron markers. Based on the prevalent expression of the Glutamate decarboxylase genes *GAD1* and *GAD2*, the neuronal population generated seems to be enriched of GABAergic inhibitory neurons. Furthermore, we compared gene expression in mutant and isogenic cells, and we observed a statistically significant difference in *GAD1*, *GAD2* and *NMDAR1* mRNA expression. In particular, the mutant cells showed the most significant reduction in the expression of *GAD1* and to a lesser extent of *GAD2* and *NMDAR1* compared with the corrected

cells. The enzyme glutamic acid decarboxylase catalyses the production of γ-aminobutyric acid (GABA) and several neurological disorders, including epilepsy, have been related with the presence of antibodies directed against GAD (118,119). Interestingly, an alteration of the GABAergic pathway was also observed in the *Cdkl5* E364X knock-in mouse model, with evidence of lower expression of the GABA receptor subunit *Gabra5* (gamma-aminobutyric acid type A receptor subunit alpha5) transcript in the brain of homozygous females in comparison with wild type mice (unpublished data). Changes in expression of these receptors have been implicated in neurological and psychiatric disorders characterized by alterations of the excitation to inhibition balance, such as epilepsy and autism spectrum disorders (120,121).

In order to assess the impact of HDR correction on *CDKL5* expression, we assayed the protein levels of CDKL5 in mutant and corrected isogenic neurons.
The E364X mutation creates a premature termination codon (PTC) that is predicted to generate a truncated CDKL5 protein lacking a large part of the C-terminal region. An alternative possibility would be the incorporation of random amino acids at the PTC in a process called read-through. This process, however, is highly dependent on the identity of the stop codon and the surrounding sequence. In the specific case, the E364X mutant harbours a UAA premature stop codon that is often considered the least permissive for a read-through (16). Besides, even if translational read-through of the PTC took place, the amino acid incorporated at the PTC might differ from the one encoded by the wild type protein, therefore leading to a missense mutation and to a mutant product.
Western blot analysis of neurons confirmed the rescue of CDKL5 protein in gene-corrected neurons, and the absence of the full-length protein in the mutant cells. It was not possible to detect the presence of truncated proteins or smaller size fractions. Therefore, at the moment, it is unknown whether the mutant results in the presence of small size truncated non-functional or functionally abnormal CDKL5 protein or in its complete absence. It's reasonable to assume that the mutated transcripts are likely to be unstable due to nonsense mediated mRNA decay process (84). NMD is a cellular surveillance pathway that reduces gene expression by eliminating mRNA transcripts containing premature PTCs (122). The ability to discriminate PTC-containing mRNA in mammalians from mRNAs with normal termination codons is dependent on the position of the PTC within the mRNA. PTC not located in the last exon and situated more than ≥ 50–55 bp upstream of the last exon-exon junction are considered NMD-triggering (123). Accordingly, our mutant *CDKL5* allele is expected to be transcribed into a transcript with an NMD-triggering PTC, and it is therefore likely to impede the expression of the encoded protein. To verify our hypothesis, we evaluated the expression of *CDKL5* at the mRNA level in mutant and corrected neural cells. The expression analysis demonstrated a decrease of *CDKL5* mRNA in the mutant line compared with the corrected one. This result suggests that *CDKL5* mRNA levels are reduced by the presence of the c.1090G>T variant, indicating that it might have a specific effect on the degradation of *CDKL5* mRNA due to the NMD process. Therefore, it is tempting to speculate that NMD could be one of the responsible mechanisms for the degradation of aberrant *CDKL5.*
Taken together, our findings have shown that precise genome editing in human cell model is possible using CRISPR/Cas9. This analysis provides an important proof of principle for genomic modifications in *in vitro* models of CDD.

Conclusion

In conclusion, our study provides evidence that CRISPR/Cas9 genome editing technology can be successfully used to target and repair a pathogenic variant in *CDKL5* (c.1090G>T (p.Glu364*)) in a patient-specific cell model.

In summary, we have developed and tested two approaches for the correction of a premature stop codon in *CDKL5*, using CRISPR/Cas9 genome editing technology, in order to expedite the discovery of new therapies for CDD.
To do so, we established dermal fibroblast and iPSC models derived from the affected individual, suitable for testing the CRISPR system *in vitro*. The initial plasmid-based approach proved to be up to 66% efficient in patient-derived fibroblasts. It was however associated to extremely variable and unpredictable editing efficiency. Therefore, we developed an alternative RNP-based approach by which we achieved targeted genome manipulation in iPSCs allowing for generation of an isogenic gene-corrected cell line that could be used as a very specific control.
Finally, through parallel differentiation of mutant and isogenic sets of cells into neural cells we demonstrated that correction of the mutation at the DNA level rescues CDKL5 protein expression and increase *CDKL5* mRNA expression in isogenic neurons.

Further studies will be needed to investigate whether the correction of the pathogenic variant restore the full functionality of CDKL5, by analysis of the phosphorylation level and the catalytic activity of CDKL5. Functional characterization of the restored CDKL5 protein could also provide more knowledge of CDKL5 functions, yet to be fully elucidated. Future research will also aim to develop *in vivo* delivery systems for the components of CRISPR/Cas9 for achievement of our ultimate goal of providing affected patients with effective therapies for CDD.

Bibliography

1. Hanefeld F. The clinical pattern of the rett syndrome. Brain Dev. 1985 Jan;7(3):320–5.

2. Goutières F, Aicardi J, Opitz JM, Reynolds JF. Atypical forms of rett syndrome. Am J Med Genet. 1986;25(S1):183–94.

3. Smeets EEJ, Pelc K, Dan B. Rett Syndrome. Mol Syndromol. 2012 Apr;2(3–5):113–27.

4. Neul JL, Kaufmann WE, Glaze DG, Christodoulou J, Clarke AJ, Bahi-Buisson N, et al. Rett Syndrome: Revised Diagnostic Criteria and Nomenclature. Ann Neurol. 2010 Dec;68(6):944–50.

5. Bahi-Buisson N, Nectoux J, Rosas-Vargas H, Milh M, Boddaert N, Girard B, et al. Key clinical features to identify girls with CDKL5 mutations. Brain. 2008 Oct 1;131(10):2647–61.

6. Fehr S, Wong K, Chin R, Williams S, de Klerk N, Forbes D, et al. Seizure variables and their relationship to genotype and functional abilities in the CDKL5 disorder. Neurology. 2016 Nov 22;87(21):2206–13.

7. Fehr S, Downs J, Ho G, de Klerk N, Forbes D, Christodoulou J, et al. Functional abilities in children and adults with the CDKL5 disorder. Am J Med Genet A. 2016 Nov;170(11):2860–9.

8. Olson HE, Demarest ST, Pestana-Knight EM, Swanson LC, Iqbal S, Lal D, et al. Cyclin-Dependent Kinase-Like 5 Deficiency Disorder: Clinical Review. Pediatr Neurol. 2019 Aug 1;97:18–25.

9. Kalscheuer VM, Tao J, Donnelly A, Hollway G, Schwinger E, Kübart S, et al. Disruption of the Serine/Threonine Kinase 9 Gene Causes Severe X-Linked Infantile Spasms and Mental Retardation. Am J Hum Genet. 2003 Jun;72(6):1401–11.

10. Weaving LS, Christodoulou J, Williamson SL, Friend KL, McKenzie OLD, Archer H, et al. Mutations of CDKL5 Cause a Severe Neurodevelopmental Disorder with Infantile Spasms and Mental Retardation. Am J Hum Genet. 2004 Dec;75(6):1079–93.

11. Scala E, Ariani F, Mari F, Caselli R, Pescucci C, Longo I, et al. CDKL5/STK9 is mutated in Rett syndrome variant with infantile spasms. J Med Genet. 2005 Feb;42(2):103–7.

12. Fehr S, Wilson M, Downs J, Williams S, Murgia A, Sartori S, et al. The CDKL5 disorder is an independent clinical entity associated with early-onset encephalopathy. Eur J Hum Genet. 2013 Mar;21(3):266–73.

13. Kothur K, Holman K, Farnsworth E, Ho G, Lorentzos M, Troedson C, et al. Diagnostic yield of targeted massively parallel sequencing in children with epileptic encephalopathy. Seizure. 2018 Jul;59:132–40.

14. Lindy AS, Stosser MB, Butler E, Downtain-Pickersgill C, Shanmugham A, Retterer K, et al. Diagnostic outcomes for genetic testing of 70 genes in 8565 patients with epilepsy and neurodevelopmental disorders. Epilepsia. 2018 May;59(5):1062–71.

15. Bahi-Buisson N, Villeneuve N, Caietta E, Jacquette A, Maurey H, Matthijs G, et al. Recurrent mutations in the CDKL5 gene: genotype-phenotype relationships. Am J Med Genet A. 2012 Jul;158A(7):1612–9.

16. Fazzari M, Frasca A, Bifari F, Landsberger N. Aminoglycoside drugs induce efficient read-through of CDKL5 nonsense mutations, slightly restoring its kinase activity. RNA Biol. 2019 Jun 23;16(10):1414–23.

17. Jakimiec M, Paprocka J, Śmigiel R. CDKL5 Deficiency Disorder—A Complex Epileptic Encephalopathy. Brain Sci. 2020 Feb 17;10(2):107.

18. Hector RD, Dando O, Landsberger N, Kilstrup-Nielsen C, Kind PC, Bailey MES, et al. Characterisation of CDKL5 Transcript Isoforms in Human and Mouse. PloS One. 2016;11(6):e0157758.

19. Kilstrup-Nielsen C, Rusconi L, La Montanara P, Ciceri D, Bergo A, Bedogni F, et al. What We Know and Would Like to Know about CDKL5 and Its Involvement in Epileptic Encephalopathy. Neural Plast. 2012 Jun 17;2012:e728267.

20. Williamson SL, Giudici L, Kilstrup-Nielsen C, Gold W, Pelka GJ, Tam PPL, et al. A novel transcript of cyclin-dependent kinase-like 5 (CDKL5) has an alternative C-terminus and is the predominant transcript in brain. Hum Genet. 2012 Feb;131(2):187–200.

21. Rusconi L, Salvatoni L, Giudici L, Bertani I, Kilstrup-Nielsen C, Broccoli V, et al. CDKL5 Expression Is Modulated during Neuronal Development and Its Subcellular Distribution Is Tightly Regulated by the C-terminal Tail. J Biol Chem. 2008 Oct 31;283(44):30101–11.

22. Bertani I, Rusconi L, Bolognese F, Forlani G, Conca B, De Monte L, et al. Functional consequences of mutations in CDKL5, an X-linked gene involved in infantile spasms and mental retardation. J Biol Chem. 2006 Oct 20;281(42):32048–56.

23. Lin C, Franco B, Rosner MR. CDKL5/Stk9 kinase inactivation is associated with neuronal developmental disorders. Hum Mol Genet. 2005 Dec 15;14(24):3775–86.

24. Montini E, Andolfi G, Caruso A, Buchner G, Walpole SM, Mariani M, et al. Identification and Characterization of a Novel Serine– Threonine Kinase Gene from the Xp22 Region. Genomics. 1998 Aug 1;51(3):427–33.

25. Katayama S, Sueyoshi N, Inazu T, Kameshita I. Cyclin-Dependent Kinase-Like 5 (CDKL5): Possible Cellular Signalling Targets and Involvement in CDKL5 Deficiency Disorder. Neural Plast. 2020;2020:6970190.

26. Hanks SK, Hunter T. Protein kinases 6. The eukaryotic protein kinase superfamily: kinase (catalytic) domain structure and classification. FASEB J Off Publ Fed Am Soc Exp Biol. 1995 May;9(8):576–96.

27. Fuchs C, Trazzi S, Torricella R, Viggiano R, De Franceschi M, Amendola E, et al. Loss of CDKL5 impairs survival and dendritic growth of newborn neurons by altering AKT/GSK-3β signaling. Neurobiol Dis. 2014 Oct;70:53–68.

28. Ricciardi S, Ungaro F, Hambrock M, Rademacher N, Stefanelli G, Brambilla D, et al. CDKL5 ensures excitatory synapse stability by reinforcing NGL-1-PSD95 interaction in the postsynaptic compartment and is impaired in patient iPSC-derived neurons. Nat Cell Biol. 2012 Sep;14(9):911–23.

29. Zhu Y-C, Li D, Wang L, Lu B, Zheng J, Zhao S-L, et al. Palmitoylation-dependent CDKL5–PSD-95 interaction regulates synaptic targeting of CDKL5 and dendritic spine development. Proc Natl Acad Sci U S A. 2013 May 28;110(22):9118–23.

30. Zhu Y-C, Xiong Z-Q. Molecular and Synaptic Bases of CDKL5 Disorder. Dev Neurobiol. 2019 Jan;79(1):8–19.

31. Ricciardi S, Kilstrup-Nielsen C, Bienvenu T, Jacquette A, Landsberger N, Broccoli V. CDKL5 influences RNA splicing activity by its association to the nuclear speckle molecular machinery. Hum Mol Genet. 2009 Dec 1;18(23):4590–602.

32. Rosas-Vargas H, Bahi-Buisson N, Philippe C, Nectoux J, Girard B, N'Guyen Morel MA, et al. Impairment of CDKL5 nuclear localisation as a cause for severe infantile encephalopathy. J Med Genet. 2008 Mar;45(3):172–8.

33. Nemos C, Lambert L, Giuliano F, Doray B, Roubertie A, Goldenberg A, et al. Mutational spectrum of CDKL5 in early-onset encephalopathies: a study of a large collection of French patients and review of the literature. Clin Genet. 2009 Oct;76(4):357–71.

34. Lykke-Andersen S, Jensen TH. Nonsense-mediated mRNA decay: an intricate machinery that shapes transcriptomes. Nat Rev Mol Cell Biol. 2015 Nov;16(11):665–77.

35. Fatscher T, Boehm V, Gehring NH. Mechanism, factors, and physiological role of nonsense-mediated mRNA decay. Cell Mol Life Sci. 2015 Dec 1;72(23):4523–44.

36. Rothstein RJ. One-step gene disruption in yeast. Methods Enzymol. 1983;101:202–11.

37. Scherer S, Davis RW. Replacement of chromosome segments with altered DNA sequences constructed in vitro. Proc Natl Acad Sci U S A. 1979 Oct;76(10):4951–5.

38. Smithies O, Gregg RG, Boggs SS, Koralewski MA, Kucherlapati RS. Insertion of DNA sequences into the human chromosomal beta-globin locus by homologous recombination. Nature. 1985 Sep 19;317(6034):230–4.

39. Thomas KR, Folger KR, Capecchi MR. High frequency targeting of genes to specific sites in the mammalian genome. Cell. 1986 Feb 14;44(3):419–28.

40. Carroll D. Genome Engineering with Targetable Nucleases. Annu Rev Biochem. 2014 Jun 2;83(1):409–39.

41. Ishino Y, Shinagawa H, Makino K, Amemura M, Nakata A. Nucleotide sequence of the iap gene, responsible for alkaline phosphatase isozyme conversion in Escherichia coli, and identification of the gene product. J Bacteriol. 1987 Dec;169(12):5429–33.

42. Jinek M, Chylinski K, Fonfara I, Hauer M, Doudna JA, Charpentier E. A programmable dual RNA-guided DNA endonuclease in adaptive bacterial immunity. Science. 2012 Aug 17;337(6096):816–21.

43. Barrangou R, Fremaux C, Deveau H, Richards M, Boyaval P, Moineau S, et al. CRISPR Provides Acquired Resistance Against Viruses in Prokaryotes. Science. 2007 Mar 23;315(5819):1709–12.

44. Carroll D. Genome Editing: Past, Present, and Future. Yale J Biol Med. 2017 Dec 19;90(4):653–9.

45. Doudna JA, Charpentier E. The new frontier of genome engineering with CRISPR-Cas9. Science. 2014 Nov 28;346(6213):1258096.

46. Makarova KS, Wolf YI, Koonin EV. The basic building blocks and evolution of CRISPR–Cas systems. Biochem Soc Trans. 2013 Dec;41(6):1392–400.

47. Cong L, Ran FA, Cox D, Lin S, Barretto R, Habib N, et al. Multiplex Genome Engineering Using CRISPR/Cas Systems. Science. 2013 Feb 15;339(6121):819–23.

48. Mali P, Yang L, Esvelt KM, Aach J, Guell M, DiCarlo JE, et al. RNA-Guided Human Genome Engineering via Cas9. Science [Internet]. 2013 Feb 15 [cited 2022 Jan 7]; Available from: https://www.science.org/doi/abs/10.1126/science.1232033

49. Choi PS, Meyerson M. Targeted genomic rearrangements using CRISPR/Cas technology. Nat Commun. 2014 Apr 24;5:3728.

50. Torres R, Martin MC, Garcia A, Cigudosa JC, Ramirez JC, Rodriguez-Perales S. Engineering human tumour-associated chromosomal translocations with the RNA-guided CRISPR-Cas9 system. Nat Commun. 2014 Jun 3;5:3964.

51. Xue W, Chen S, Yin H, Tammela T, Papagiannakopoulos T, Joshi NS, et al. CRISPR-mediated direct mutation of cancer genes in the mouse liver. Nature. 2014 Oct 16;514(7522):380–4.

52. Wang G, McCain ML, Yang L, He A, Pasqualini FS, Agarwal A, et al. Modeling the mitochondrial cardiomyopathy of Barth syndrome with induced pluripotent stem cell and heart-on-chip technologies. Nat Med. 2014 Jun;20(6):616–23.

53. Claussnitzer M, Dankel SN, Kim K-H, Quon G, Meuleman W, Haugen C, et al. FTO Obesity Variant Circuitry and Adipocyte Browning in Humans. N Engl J Med. 2015 Sep 3;373(10):895–907.

54. Paquet D, Kwart D, Chen A, Sproul A, Jacob S, Teo S, et al. Efficient introduction of specific homozygous and heterozygous mutations using CRISPR/Cas9. Nature. 2016 May 5;533(7601):125–9.

55. Shalem O, Sanjana NE, Hartenian E, Shi X, Scott DA, Mikkelson T, et al. Genome-scale CRISPR-Cas9 knockout screening in human cells. Science. 2014 Jan 3;343(6166):84–7.

56. Zhou Y, Zhu S, Cai C, Yuan P, Li C, Huang Y, et al. High-throughput screening of a CRISPR/Cas9 library for functional genomics in human cells. Nature. 2014 May 22;509(7501):487–91.

57. De Masi C, Spitalieri P, Murdocca M, Novelli G, Sangiuolo F. Application of CRISPR/Cas9 to human-induced pluripotent stem cells: from gene editing to drug discovery. Hum Genomics. 2020 Jun 26;14(1):25.

58. Chang C-Y, Ting H-C, Su H-L, Jeng J-R. Combining Induced Pluripotent Stem Cells and Genome Editing Technologies for Clinical Applications. Cell Transplant. 2018 Mar;27(3):379–92.

59. Hockemeyer D, Jaenisch R. Induced pluripotent stem cells meet genome editing. Cell Stem Cell. 2016 May 5;18(5):573–86.

60. Kearns NA, Genga RMJ, Enuameh MS, Garber M, Wolfe SA, Maehr R. Cas9 effector-mediated regulation of transcription and differentiation in human pluripotent stem cells. Dev Camb Engl. 2014 Jan;141(1):219–23.

61. Rong Z, Zhu S, Xu Y, Fu X. Homologous recombination in human embryonic stem cells using CRISPR/Cas9 nickase and a long DNA donor template. Protein Cell. 2014 Apr;5(4):258–60.

62. Kim S, Kim D, Cho SW, Kim J, Kim J-S. Highly efficient RNA-guided genome editing in human cells via delivery of purified Cas9 ribonucleoproteins. Genome Res. 2014 Jun;24(6):1012–9.

63. Cyranoski D. Chinese scientists to pioneer first human CRISPR trial. Nature. 2016 Jul 28;535(7613):476–7.

64. Galarreta MR de, Lujambio A. Therapeutic editing of hepatocyte genome in vivo. J Hepatol. 2017 Oct 1;67(4):818–28.

65. Frangoul H, Altshuler D, Cappellini MD, Chen Y-S, Domm J, Eustace BK, et al. CRISPR-Cas9 Gene Editing for Sickle Cell Disease and β-Thalassemia. N Engl J Med. 2021 Jan 21;384(3):252–60.

66. Lu Y, Xue J, Deng T, Zhou X, Yu K, Deng L, et al. Safety and feasibility of CRISPR-edited T cells in patients with refractory non-small-cell lung cancer. Nat Med. 2020 May;26(5):732–40.

67. Yin H, Song C-Q, Dorkin JR, Zhu LJ, Li Y, Wu Q, et al. Therapeutic genome editing by combined viral and non-viral delivery of CRISPR system components in vivo. Nat Biotechnol. 2016 Mar;34(3):328–33.

68. Abrahimi P, Chang WG, Kluger MS, Qyang Y, Tellides G, Saltzman WM, et al. Efficient gene disruption in cultured primary human endothelial cells by CRISPR/Cas9. Circ Res. 2015 Jul 3;117(2):121–8.

69. Sander JD, Joung JK. CRISPR-Cas systems for genome editing, regulation and targeting. Nat Biotechnol. 2014 Apr;32(4):347–55.

70. Liu M, Rehman S, Tang X, Gu K, Fan Q, Chen D, et al. Methodologies for Improving HDR Efficiency. Front Genet [Internet]. 2019 [cited 2022 Jan 14];9. Available from: https://www.frontiersin.org/article/10.3389/fgene.2018.00691

71. Bothmer A, Phadke T, Barrera LA, Margulies CM, Lee CS, Buquicchio F, et al. Characterization of the interplay between DNA repair and CRISPR/Cas9-induced DNA lesions at an endogenous locus. Nat Commun. 2017 Jan 9;8:13905.

72. Her J, Bunting SF. How cells ensure correct repair of DNA double-strand breaks. J Biol Chem. 2018 Jul 6;293(27):10502–11.

73. Hao M, Qiao J, Qi H. Current and Emerging Methods for the Synthesis of Single-Stranded DNA. Genes. 2020 Jan 21;11(2):116.

74. Liu C, Zhang L, Liu H, Cheng K. Delivery Strategies of the CRISPR-Cas9 Gene-Editing System for Therapeutic Applications. J Control Release Off J Control Release Soc. 2017 Nov 28;266:17–26.

75. Biagioni A, Laurenzana A, Margheri F, Chillà A, Fibbi G, Del Rosso M. Delivery systems of CRISPR/Cas9-based cancer gene therapy. J Biol Eng. 2018;12:33.

76. Li H, Yang Y, Hong W, Huang M, Wu M, Zhao X. Applications of genome editing technology in the targeted therapy of human diseases: mechanisms, advances and prospects. Signal Transduct Target Ther. 2020 Jan 3;5(1):1–23.

77. Lee K, Conboy M, Park HM, Jiang F, Kim HJ, Dewitt MA, et al. Nanoparticle delivery of Cas9 ribonucleoprotein and donor DNA in vivo induces homology-directed DNA repair. Nat Biomed Eng. 2017;1:889–901.

78. Pini G, Bigoni S, Engerström IW, Calabrese O, Felloni B, Scusa MF, et al. Variant of Rett syndrome and CDKL5 gene: clinical and autonomic description of 10 cases. Neuropediatrics. 2012 Feb;43(1):37–43.

79. Dracopoli NC, Haines JL, Korf BR. Current protocols in human genetics. 1994 Dec 31 [cited 2022 Jan 9]; Available from: https://www.osti.gov/biblio/110965

80. Cho MS, Lee Y-E, Kim JY, Chung S, Cho YH, Kim D-S, et al. Highly efficient and large-scale generation of functional dopamine neurons from human embryonic stem cells. Proc Natl Acad Sci U S A. 2008 Mar 4;105(9):3392–7.

81. Campos PB, Sartore RC, Abdalla SN, Rehen SK. Chromosomal Spread Preparation of Human Embryonic Stem Cells for Karyotyping. JoVE J Vis Exp. 2009 Sep 4;(31):e1512.

82. Auricchio A, O'Connor E, Hildinger M, Wilson JM. A single-step affinity column for purification of serotype-5 based adeno-associated viral vectors. Mol Ther J Am Soc Gene Ther. 2001 Oct;4(4):372–4.

83. Swiech L, Heidenreich M, Banerjee A, Habib N, Li Y, Trombetta J, et al. In vivo interrogation of gene function in the mammalian brain using CRISPR-Cas9. Nat Biotechnol. 2015 Jan;33(1):102–6.

84. Nectoux J, Fichou Y, Cagnard N, Bahi-Buisson N, Nusbaum P, Letourneur F, et al. Cell cloning-based transcriptome analysis in cyclin-dependent kinase-like 5 mutation patients with severe epileptic encephalopathy. J Mol Med Berl Ger. 2011 Feb;89(2):193–202.

85. Allen RC, Zoghbi HY, Moseley AB, Rosenblatt HM, Belmont JW. Methylation of HpaII and HhaI sites near the polymorphic CAG repeat in the human androgen-receptor gene correlates with X chromosome inactivation. Am J Hum Genet. 1992 Dec;51(6):1229–39.

86. Croci S, Carriero ML, Capitani K, Daga S, Donati F, Papa FT, et al. AAV-mediated FOXG1 gene editing in human Rett primary cells. Eur J Hum Genet. 2020 Oct;28(10):1446–58.

87. Croci S, Carriero ML, Capitani K, Daga S, Donati F, Frullanti E, et al. High rate of HDR in gene editing of p.(Thr158Met) MECP2 mutational hotspot. Eur J Hum Genet. 2020 Sep;28(9):1231–42.

88. Park J, Lim K, Kim J-S, Bae S. Cas-analyzer: an online tool for assessing genome editing results using NGS data. Bioinformatics. 2017 Jan 15;33(2):286–8.

89. Liang J-S, Shimojima K, Takayama R, Natsume J, Shichiji M, Hirasawa K, et al. CDKL5 alterations lead to early epileptic encephalopathy in both genders. Epilepsia. 2011 Oct;52(10):1835–42.

90. Mei D, Marini C, Novara F, Bernardina BD, Granata T, Fontana E, et al. Xp22.3 genomic deletions involving the CDKL5 gene in girls with early onset epileptic encephalopathy. Epilepsia. 2010 Apr;51(4):647–54.

91. Szafranski P, Golla S, Jin W, Fang P, Hixson P, Matalon R, et al. Neurodevelopmental and neurobehavioral characteristics in males and females with CDKL5 duplications. Eur J Hum Genet EJHG. 2015 Jul;23(7):915–21.

92. Chung C-Y, Yang J-T, Kuo Y-C. Polybutylcyanoacrylate nanoparticle-mediated neurotrophin-3 gene delivery for differentiating iPS cells into neurons. Biomaterials. 2013 Jul;34(22):5562–70.

93. Ryan SD, Dolatabadi N, Chan SF, Zhang X, Akhtar MW, Parker J, et al. Isogenic human iPSC Parkinson's model shows nitrosative stress-induced dysfunction in MEF2-PGC1α transcription. Cell. 2013 Dec 5;155(6):1351–64.

94. Wang F, Kong J, Cui Y-Y, Liu P, Wen J-Y. Is Human-induced Pluripotent Stem Cell the Best Optimal? Chin Med J (Engl). 2018 Apr 5;131(7):852–6.

95. Yusa K, Rashid ST, Strick-Marchand H, Varela I, Liu P-Q, Paschon DE, et al. Targeted gene correction of α1-antitrypsin deficiency in induced pluripotent stem cells. Nature. 2011 Oct 12;478(7369):391–4.

96. Goto T, Monk M. Regulation of X-chromosome inactivation in development in mice and humans. Microbiol Mol Biol Rev MMBR. 1998 Jun;62(2):362–78.

97. Tchieu J, Kuoy E, Chin MH, Trinh H, Patterson M, Sherman SP, et al. Female human iPS cells retain an inactive X-chromosome. Cell Stem Cell. 2010 Sep 3;7(3):329–42.

98. Silva SS, Rowntree RK, Mekhoubad S, Lee JT. X-chromosome inactivation and epigenetic fluidity in human embryonic stem cells. Proc Natl Acad Sci U S A. 2008 Mar 25;105(12):4820–5.

99. Ananiev G, Williams EC, Li H, Chang Q. Isogenic pairs of wild type and mutant induced pluripotent stem cell (iPSC) lines from Rett syndrome patients as in vitro disease model. PloS One. 2011;6(9):e25255.

100. Marchetto MCN, Carromeu C, Acab A, Yu D, Yeo GW, Mu Y, et al. A model for neural development and treatment of Rett syndrome using human induced pluripotent stem cells. Cell. 2010 Nov 12;143(4):527–39.

101. Pattanayak V, Lin S, Guilinger JP, Ma E, Doudna JA, Liu DR. High-throughput profiling of off-target DNA cleavage reveals RNA-programmed Cas9 nuclease specificity. Nat Biotechnol. 2013 Sep;31(9):839–43.

102. Chong ZX, Yeap SK, Ho WY. Transfection types, methods and strategies: a technical review. PeerJ. 2021 Apr 21;9:e11165.

103. Symington LS, Gautier J. Double-Strand Break End Resection and Repair Pathway Choice. Annu Rev Genet. 2011 Dec 15;45(1):247–71.

104. Chang J, Chen X, Zhang T, Wang R, Wang A, Lan X, et al. The novel insight into the outcomes of CRISPR/Cas9 editing intra- and inter-species. Int J Biol Macromol. 2020 Nov;163:711–7.

105. Hinz JM, Laughery MF, Wyrick JJ. Nucleosomes Inhibit Cas9 Endonuclease Activity in Vitro. Biochemistry. 2015 Dec 8;54(48):7063–6.

106. Liu G, Yin K, Zhang Q, Gao C, Qiu J-L. Modulating chromatin accessibility by transactivation and targeting proximal dsgRNAs enhances Cas9 editing efficiency in vivo. Genome Biol. 2019 Jul 26;20(1):145.

107. Jensen KT, Fløe L, Petersen TS, Huang J, Xu F, Bolund L, et al. Chromatin accessibility and guide sequence secondary structure affect CRISPR-Cas9 gene editing efficiency. FEBS Lett. 2017 Jul;591(13):1892–901.

108. Liu Y, Li J, Zhou C, Meng B, Wei Y, Yang G, et al. Allele-specific genome editing of imprinting genes by preferentially targeting non-methylated loci using Staphylococcus aureus Cas9 (SaCas9). Sci Bull. 2019 Nov 15;64(21):1592–600.

109. Hsu PD, Scott DA, Weinstein JA, Ran FA, Konermann S, Agarwala V, et al. DNA targeting specificity of RNA-guided Cas9 nucleases. Nat Biotechnol. 2013 Sep;31(9):827–32.

110. Pescucci C, Meloni I, Bruttini M, Ariani F, Longo I, Mari F, et al. Chromosome 2 deletion encompassing the MAP2 gene in a patient with autism and Rett-like features: Rett-like phenotype and 2q34 deletion. Clin Genet. 2003 Nov 18;64(6):497–501.

111. Kaufmann WE, Taylor CV, Hohmann CF, Sanwal IB, Naidu S. Abnormalities in neuronal maturation in Rett syndrome neocortex: preliminary molecular correlates. Eur Child Adolesc Psychiatry. 1997;6 Suppl 1:75–7.

112. Colantuoni C, Jeon OH, Hyder K, Chenchik A, Khimani AH, Narayanan V, et al. Gene expression profiling in postmortem Rett Syndrome brain: differential gene expression and patient classification. Neurobiol Dis. 2001 Oct;8(5):847–65.

113. Barbiero I, Bianchi M, Kilstrup-Nielsen C. Therapeutic potential of pregnenolone and pregnenolone methyl ether on depressive and CDKL5 deficiency disorders: Focus on microtubule targeting. J Neuroendocrinol. n/a(n/a):e13033.

114. Barbiero I, De Rosa R, Kilstrup-Nielsen C. Microtubules: A Key to Understand and Correct Neuronal Defects in CDKL5 Deficiency Disorder? Int J Mol Sci. 2019 Aug 21;20(17):4075.

115. Eng LF. Glial fibrillary acidic protein (GFAP): the major protein of glial intermediate filaments in differentiated astrocytes. J Neuroimmunol. 1985;8:203–14.

116. Conti F. Localization of NMDA receptors in the cerebral cortex: a schematic overview. Braz J Med Biol Res. 1997 May;30:555–60.

117. Perez-Rando M, Castillo-Gómez E, Guirado R, Blasco-Ibañez JM, Crespo C, Varea E, et al. NMDA Receptors Regulate the Structural Plasticity of Spines and Axonal Boutons in Hippocampal Interneurons. Front Cell Neurosci [Internet]. 2017 [cited 2022 Feb 24];11. Available from: https://www.frontiersin.org/article/10.3389/fncel.2017.00166

118. Baizabal-Carvallo JF. The neurological syndromes associated with glutamic acid decarboxylase antibodies. J Autoimmun. 2019 Jul;101:35–47.

119. Vianello M, Tavolato B, Giometto B. Glutamic acid decarboxylase autoantibodies and neurological disorders. Neurol Sci. 2002 Oct 1;23(4):145–51.

120. Fatemi SH, Folsom TD. GABA receptor subunit distribution and FMRP-mGluR5 signaling abnormalities in the cerebellum of subjects with schizophrenia, mood disorders, and autism. Schizophr Res. 2015 Sep;167(1–3):42–56.

121. Kaila K, Ruusuvuori E, Seja P, Voipio J, Puskarjov M. GABA actions and ionic plasticity in epilepsy. Curr Opin Neurobiol. 2014 Jun;26:34–41.

122. Schweingruber C, Rufener SC, Zünd D, Yamashita A, Mühlemann O. Nonsense-mediated mRNA decay - mechanisms of substrate mRNA recognition and degradation in mammalian cells. Biochim Biophys Acta. 2013 Jul;1829(6–7):612–23.

123. Kurosaki T, Maquat LE. Nonsense-mediated mRNA decay in humans at a glance. J Cell Sci. 2016 Feb 1;129(3):461–7.

IDIBELL
Institut d'Investigació Biomèdica de Belvitge

P-CMR[C]

Dr. Palmieri Maria, PhD
Scientific Secretary, Doctorate GenOMeC
University of Siena, 53100 - Siena - Italy
Email: doctorate.genomec@dbm.unisi.it

RE: PhD thesis evaluation - Miriam Lucia Carriero

February 10, 2022

Dear Dr. Palmieri,

As per your kind request, I have now completed the thorough perusal of the PhD thesis proposal "*CRISPR/Cas9-based targeted genome editing for the treatment of CDKL5 deficiency disorder*", submitted by doctoral candidate Ms. Miriam Lucia Carriero.

This thesis describes the generation and validation of an induced pluripotent stem cell (iPSC)-based model of CDKL5 deficiency consisting of patient-specific, genetically corrected isogenic iPSC. The candidate presents a succinct, yet sufficiently informative, background on the disease caused by CDKL5 deficiency, as well as on the methodological concepts underlying iPSC-based disease modeling and CRISPR/Cas9-based genome edition. The methodology employed for genome edition is state-of-the-art and includes nucleofection of ribonucleoprotein complexes and the use of short single-stranded DNA oligonucleotides as templates for recombination. The results are described with clarity; efficiencies are consistent with proper implementation of CRISPR/Cas9 technology, and the validation studies demonstrate successful recovery of functional wild-type CDKL5 expression in iPSC-derived neurons. I did not find any sections of the thesis where significant additions or corrections were needed.

For these reasons, I consider the PhD thesis proposal "*CRISPR/Cas9-based targeted genome editing for the treatment of CDKL5 deficiency disorder*", submitted by doctoral candidate Ms. Miriam Lucia Carriero, to be a good thesis and hereby agree to admit the candidate to the defense.

Yours sincerely,

RAYA CHAMORRO ANGEL - 29157851S

Digitally signed by RAYA CHAMORRO ANGEL - 29157851S
Date: 2022.02.14 11:58:20 +01'00'

Angel Raya, MD, PhD
ICREA Research Professor
Coordinator,
Regenerative Medicine Program,
Bellvitge Biomedical Research Institute (IDIBELL)
Director,
Program for Clinical Translation of Regenerative Medicine in Catalonia (P-CMR[C])

Bellvitge Biomedical Research Institute (IDIBELL) | Program for Clinical Translation of Regenerative Medicine in Catalonia–P-CMR[C]
Hospital Duran i Reynals – 3rd floor | Av. Gran Via 199-203 | 08908 Hospitalet de Llobregat (Barcelona) | Spain
Tel +34 93 316 03 21 | Email: araya@idibell.cat | www.idibell.cat | www.p-cmrc.cat

UNIVERSITÀ DI TORINO
DIPARTIMENTO DI NEUROSCIENZE
"RITA LEVI MONTALCINI"

MAURIZIO GIUSTETTO, PHD
ASSOCIATE PROFESSOR OF HUMAN ANATOMY

Torino, 16.02.2022

To the faculty members of Doctorate GenOMeC

University of Siena, Policlinico S Maria alle Scotte

Re: Evaluation of Miriam Lucia Carriero's thesis "CRISPR/Cas9-based targeted genome editing for the treatment of Cdkl5 deficiency disorder"

To whom it may concern: I would like to express my deep congratulations to the PhD candidate because the scientific work presented in this Thesis represents an important piece of work that will benefit the field of precision medicine, especially for neurodevelopmental disorders.

The thesis is well written and clear, the English language is excellent.

However, the comments that I inserted into the PDF file of the Thesis shall improve the text and the interpretation of the results. In particular, I would like to mention that the Introduction section could be written with more details on the neurobiological consequences of CDD, both those reported in mice models and, especially, those recently published on iPSC-derived neurons/organoids from CDD patients' tissues. Finally, Intro section could be more punchy/incisive if images will be added on the Crispr/CAS9 technology and with some more clarification in the relative paragraphs.

Finally, I deem that Miriam Lucia Carriero has brilliantly fulfilled the admission requirements for the final Thesis defense session.

Faithfully,

Prof. Maurizio Giustetto

Maurizio Giustetto - email: maurizio.giustetto@unito.it
C.so Raffaello, 30 - 10126 TORINO (Italia) Telefono: 011 - 670.7725/22 - fax 011 - 670.5931